

# THESIS REPORT

Master's Degree

## Optimization of Machining Performance of Dental Ceramic Restorative Materials

*by D.T. Le*

*Advisor: G. Zhang*

M.S. 97-1



*Sponsored by  
the National Science Foundation  
Engineering Research Center Program,  
the University of Maryland,  
Harvard University,  
and Industry*

## **Abstract**

Title of Thesis:       OPTIMIZATION OF MACHINING PERFORMANCE OF  
                              DENTAL CERAMIC RESTORATIVE MATERIALS

Degree candidate:     Dung Thanh Le

Degree and year:      Master of Science, 1997

Thesis directed by:   Associate Professor Guangming Zhang  
                              Department of Mechanical Engineering  
                              & Institute for Systems Research

Dental ceramics are gaining popularity because of their esthetics, strength, chemical durability, and bio-compatibility. However, the inherent brittleness of ceramics poses a challenge to the manufacturing community as the cracking formed during the material removal leads to premature clinical failures. Consequently, fabrication of excellent-fitting and durable dental prostheses calls for new and innovative processing technologies to minimize the formation of micro-scale cracking.

This thesis presents a combined analytical and experimental study with focus on optimizing the machining performance of a type of newly developed dental material. It is called DICOR/MGC, where MGC stands for machinable glass ceramic. The study starts from analyzing their microstructural characteristics to searching for the machining conditions that provide satisfactory performance in terms of surface finish and acceptable flexural strength. To gain a better understanding of the material removal mechanism(s), a dynamometer is designed to

perform an on-line recording of the cutting force generated during machining. Method of using an environmental scanning electron microscope is employed to examine the machined surface texture and identify the machining induced cracking.

Two major contributions of this thesis study are (1) the fundamental understanding of the relationships among the material microstructures, the machining parameters, and the material preparation on surface integrity of dental ceramics, and (2) the development of an architecture for searching machining conditions that optimize the machining performance of dental ceramics.

**OPTIMIZATION OF MACHINING PERFORMANCE OF DENTAL CERAMIC  
RESTORATIVE MATERIALS**

by

Dung Thanh Le

Thesis submitted to the Faculty of the Graduate School of the  
University of Maryland at College Park in partial fulfillment  
of the requirements for the degree of  
Master of Science  
1997

Advisory Committee:

Associate Professor Guangming Zhang, Chairman/Advisor  
Professor William L. Fournery  
Professor Edward B. Magrab

## **Dedication**

To my family

## Acknowledgments

This thesis represents work that was accumulated over a period of two years, with help from many professors, fellow graduate and undergraduate students, and staff members. I am indebted for the time, support, and ideas of everyone.

Special thanks go to all past and current lab members at the Advanced Design and Manufacturing Lab, including Stanley Ng, Rena Surana, Huynh Luu, Lixun Qi, Shelly Tucker, Melvin Jung, Adrian Hood, Charles Clinton, Mark Richardson, Lenox Job, Xin Che, and John Eshleman.

For the wonderful support from the Mechanical Engineering Department, I would like to thank the following people: Mr. David Hahn, for his assistance with testing equipment and technical advice; Mr. Gene Taylor and Dr. Mary Li, for their expert training and advice on the use of the environmental scanning electron microscope; and Ms. Brown, for her processing of all those purchase requests.

For serving on the thesis committee and helping to revise the thesis, I would like to thank Professors Fourney and Magrab, whose comments and suggestions have helped to elucidate the ideas in this thesis.

For providing the financial support over the last two years, I would like to commend the NIH Machinable Ceramics Grant of the opportunity. The experience of working on a multi-disciplinary team has been very rewarding.

Finally, I would like to express my deep gratitude to Dr. Guangming Zhang, my program advisor. His dedication to and encouragement of my work has been invaluable to the completion of this thesis. I am truly grateful.

## Table of Contents

|   |             |
|---|-------------|
| <b>Dedication .....</b>   | <b>ii</b>   |
| <b>Acknowledgments .....</b>  | <b>iii</b>  |
| <b>List of Tables .....</b>   | <b>vii</b>  |
| <b>List of Figures .....</b>  | <b>viii</b> |
| <br>  |             |
| <b>1 Introduction .....</b>   | <b>1</b>    |
| 1.1 Background .....  | 1           |
| 1.2 Machining Performance of Dental Ceramics .....                      | 3           |
| 1.3 Scope of the Thesis .....   | 6           |
| 1.4 Organization of the Thesis .....                                    | 8           |
| <br>  |             |
| <b>2 Literature Review .....</b>  | <b>9</b>    |
| 2.1 Traditional and Advanced Ceramics .....                             | 9           |
| 2.2 Machining of Ceramics .....   | 11          |
| 2.3 Dental Glass Ceramics .....   | 18          |
| 2.4 Machinability .....   | 20          |
| 2.5 Ceramic Microstructures .....                                       | 22          |
| <br>  |             |
| <b>3 Architecture for the Optimizing of Machining Performance .....</b> | <b>25</b>   |
| 3.1 Characterization of Microstructure .....                            | 26          |

|          |  |           |
|----------|--|-----------|
| 3.2      | Identification of Machining Parameters .....                           | 27        |
| 3.3      | On-line Monitoring of the Machining Operations .....                   | 28        |
| 3.4      | Evaluation of Machining Performance .....                              | 29        |
| <b>4</b> | <b>Characterization of the Microstructure of Dental Ceramics .....</b> | <b>30</b> |
| 4.1      | Experimental Methodology .....   | 30        |
| 4.2      | ESEM/Computer-Based System .....                                       | 32        |
| 4.3      | Microstructural Analysis .....   | 33        |
| <b>5</b> | <b>Design and Fabrication of a Dynamometer .....</b>                   | <b>36</b> |
| 5.1      | Strain Gages .....   | 36        |
| 5.2      | Wheatstone Bridge .....  | 39        |
| 5.2.1    | Bridge Equations .....   | 39        |
| 5.2.2    | Bridge Configurations .....  | 42        |
| 5.3      | Sensing Element .....  | 43        |
| 5.4      | The Dynamometer .....  | 46        |
| 5.4.1    | Components of the Dynamometer .....                                    | 47        |
| 5.4.2    | Estimation of the Natural Frequency .....                              | 50        |
| 5.5      | Data Acquisition System .....  | 51        |
| 5.6      | Calibration .....  | 54        |
| 5.7      | Calibration .....  | 48        |
| <b>6</b> | <b>Evaluation of Machining Performance .....</b>                       | <b>57</b> |
| 6.1      | Procedure .....  | 57        |



|          |  |           |
|----------|--|-----------|
| 6.2      | Experimental Data .....  | 61        |
| 6.2.1    | Cutting Forces .....   | 61        |
| 6.2.2    | Fracture Strength Measurements .....   | 62        |
| 6.3      | Data Analysis and Discussion of Results .....  | 66        |
| 6.3.1    | Relation Between Cutting Force and Strength Degradation ....                                       | 66        |
| 6.3.2    | Empirical Models Relating the Cutting Force<br>to Machining Conditions .....                       | 68        |
| 6.3.3    | The Effects of Microstructure on Cutting Forces,<br>Flexural Strength, and Surface Integrity ..... | 72        |
| <b>7</b> | <b>Conclusions and Recommendations .....</b>   | <b>78</b> |
| 7.1      | Conclusions .....  | 78        |
| 7.2      | Recommendations .....  | 80        |
|          | <b>Appendices .....</b>  | <b>82</b> |
| A        | ESEM Micrographs of Microstructures .....  | 82        |
| B        | ESEM Micrographs of Machined DICOR/MGC .....   | 85        |
|          | <b>References .....</b>  | <b>92</b> |

## List Of Tables

|           |   |    |
|-----------|---|----|
| Table 2-1 | Advanced ceramic functions, properties, and applications .....  | 10 |
| Table 2-2 | Some mechanical properties of DICOR/MGC .....   | 20 |
| Table 2-3 | Types of short-term machinability tests .....   | 22 |
| Table 4-1 | Microstructural features of DICOR/MGC .....   | 35 |
| Table 5-1 | Components of the dynamometer .....   | 48 |
| Table 5-2 | DAQ system characteristics .....  | 53 |
| Table 5-3 | Variation of the cutting force due to specimen location .....   | 55 |
| Table 6-1 | High and low settings for the machining parameters .....  | 59 |
| Table 6-2 | Design Matrix .....   | 59 |
| Table 6-3 | Cutting Force Measurement Data .....  | 63 |
| Table 6-4 | Fracture Strength Measurement Data .....  | 65 |
| Table 6-5 | Main and interaction effects of machining<br>parameters on the cutting force .....                          | 69 |
| Table 6-6 | Data points for normal probability plot for DICOR/MGC-Fine ....   | 70 |
| Table 6-7 | 8-test averages and standard deviations from force and<br>flexural strength measurements of DICOR/MGC ..... | 73 |

## List Of Figures

|            |   |    |
|------------|---|----|
| Figure 1-1 | Sequence of CAD/CAM systems on dental ceramics and the degradation in mechanical properties after machining ..... | 4  |
| Figure 2-1 | Dependence of material removal mechanism on machining conditions .....  | 12 |
| Figure 2-2 | A five-stage process in the material removal mechanism of ceramics .....  | 14 |
| Figure 2-3 | Two types of chips observed in the machining of ceramics .....  | 15 |
| Figure 2-4 | An end milling operation defined by three parameters .....  | 17 |
| Figure 2-5 | Dental ceramic materials for restorations .....   | 18 |
| Figure 2-6 | Comparison of flexural strengths of existing dental ceramics .....  | 19 |
| Figure 2-7 | Ceramic microstructural features .....  | 23 |
| Figure 3-1 | Flowchart of the optimization architecture .....  | 25 |
| Figure 3-2 | Contribution of the machining parameters to the cutting process, surface roughness, and force generation .....    | 28 |
| Figure 3-3 | Components of the evaluation of machining performance .....   | 29 |
| Figure 4-1 | Procedure for analyzing microstructures .....   | 31 |
| Figure 4-2 | ESEM/Computer-based system for microstructural analysis .....   | 32 |
| Figure 4-3 | Microstructures of Dental Ceramics .....  | 34 |
| Figure 5-1 | An example of a foil strain gage .....  | 38 |
| Figure 5-2 | Circuit configuration of a full Wheatstone bridge .....   | 40 |
| Figure 5-3 | Sensing element: (a) strain gage configuration and (b) sectional view .....                                       | 44 |

|             |  |    |
|-------------|--|----|
| Figure 5-4  | Strain response of (a) a hollow cylinder and (b) a cantilever .....  | 44 |
| Figure 5-5  | The strain gages in Figure 5-3 are shown in their bridge configurations .....                                | 45 |
| Figure 5-6  | Dynamometer shown during a machining experiment .....  | 46 |
| Figure 5-7  | Overall dimensions of the dynamometer .....  | 47 |
| Figure 5-8  | Details of the top components of the dynamometer .....   | 49 |
| Figure 5-9  | Dynamometer represented by spring-mass system .....  | 50 |
| Figure 5-10 | Computer with LabVIEW running and signal conditioning module .....   | 51 |
| Figure 5-11 | Components of the data acquisition (DAQ) system .....  | 52 |
| Figure 5-12 | Plots showing variation of measured cutting forces .....   | 55 |
| Figure 5-13 | Calibration results for the (a) X direction and (b) Y direction .....  | 56 |
| Figure 6-1  | Geometrical representation of the design matrix .....  | 60 |
| Figure 6-2  | Vise-fixtured system for machining .....   | 61 |
| Figure 6-3  | Example of a force signal .....  | 62 |
| Figure 6-4  | Four-Point Bending Tests to Evaluate Fracture Strength .....   | 64 |
| Figure 6-5  | Fracture strength degradation of three types of DICOR/MGC for the a) feed and b) transverse directions ..... | 68 |
| Figure 6-6  | Normal probability plot for DICOR/MGC-Fine .....   | 71 |
| Figure 6-7  | Variation of (a) cutting forces and (b) flexural strengths as a function of microstructure .....             | 73 |
| Figure 6-8  | ESEM micrographs (x250) of machined DICOR/MGC surfaces .....   | 75 |
| Figure 6-9  | Micrograph of DICOR/MGC-Coarse showing material removal mechanism .....                                      | 76 |



# Chapter 1

## Introduction

### 1.1 BACKGROUND

As industry needs continue to push the performance limits of metals, more and more research is being conducted to take advantage of the superior properties of advanced ceramics, such as higher strength-to-mass ratio, and higher resistance to severe environments like heat, wear, and corrosion. These outstanding qualifications of ceramics have led to their uses in wide-ranging applications where performance and reliability must be ensured. Yet, for all the potential that ceramics offer, the question remains in how to best process these materials. The material removal process in ceramics, unlike that of common metals and plastics, is characterized by micro-cracking and brittle fracture. Consequently, a machined ceramic part tends to possess poor surface finish and to fail at a reduced fracture strength.

Research in advanced ceramics has been on-going for decades, and has contributed to engineering advances in many fields. The research ranges from the traditional automotive and electronics industries to the newer areas of bio-medical engineering. Traditionally, high-precision grinding is used to machine ceramics to minimize the generation of surface/sub-surface damages. In this type of abrasive machining, diamond particles are used and small depths of cut are set to ensure that the generation of micro-scale cracks is under control. The abrasive machining has the benefit of minimizing the surface and sub-surface cracking induced during the

machining process. However, high-precision grinding is disadvantageous for two reasons. First, small depths of cut in high-precision grinding lead to an economically inefficient operation because production time and tooling cost are increased due to the lowered rate of material removal and the use of expensive diamond particles, respectively. Therefore, high-precision grinding is mostly useful as a finishing operation. Second, the shaping capabilities of grinding is limited in terms of what geometrical shapes can be achieved. For example, complex curved surfaces are impractical to fabricate using the grinding method, and alternative machining methods must be sought such as turning and milling.

In recent years, developments in material synthesis of ceramics have dramatically improved the machinability of ceramics. A significant amount of research has been focused on improving the mechanical and physical properties of ceramics in an effort to reduce the effects of brittleness. For example, ceramics can be made tougher by controlling the orientation and size of the grains in the microstructure to provide effective barriers against cracking [Musikant, 1991]. Consequently, glass ceramic materials have been widely used in applications where greater tolerance to brittleness is needed. The level of progress has been significant to the point where alternative machining methods beyond grinding may now be investigated.

In this thesis, conventional end milling of a new type of advanced ceramics is explored as a viable machining alternative to grinding. Efforts of this work are made to investigate the machining performance of a special type of dental ceramic material for use in restorative dentistry. Currently, a need exists in this field to improve the fabrication of dental restorations in terms of efficiency and accuracy.

Under traditional methods, restorations are crafted using the skilled hands of dentists in which neither speed nor accuracy can be guaranteed. However, with the availability of machinable glass ceramics, alternative solutions exist to improve machining productivity, accuracy, and reliability. This thesis study focuses on evaluating and optimizing the milling performance of dental ceramics.

## **1.2 MACHINING PERFORMANCE OF DENTAL CERAMICS**

Dental ceramics are ideal candidates for restorative applications because many of their characteristics -- color, texture, and mechanical properties -- closely resemble those of human teeth. However, during shaping processes, some of the mechanical properties of the dental ceramics are likely to be degraded as a result of surface/sub-surface damages. Thus it is the question of how a dental material responds to machining, i.e. its machining performance, that is more crucial in assessing the overall restorative effectiveness. To illustrate this point, in Figure 1-1, the process of fabricating dental restorations from ceramics is shown. It illustrates the four-step sequence of the manufacturing of ceramic material, computer-aided design, computer-aided manufacturing systems, and machining operations.

The performance of dental restorations relies heavily on inherent material properties and influence of the shaping process. As illustrated in Figure 1-1, before machining, a dental ceramic is characterized by certain mechanical properties, such as hardness and fracture strength which are determined mainly by its microstructure. However, after the CAD/CAM processes, in which the end product is a ceramic restoration, the mechanical properties of the material are changed due



to the introduction of surface damages such as cracking. The result is a restoration with weakened mechanical properties. Thus the machining optimization of dental ceramics poses some key questions such as how degradation of mechanical properties occurs and whether it is possible to control that degradation.

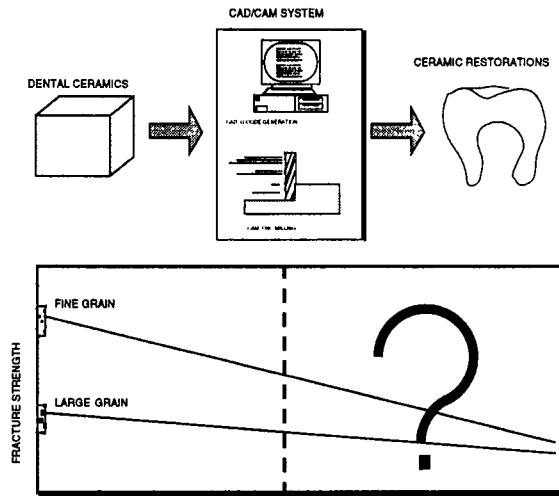


Figure 1-1. Sequence of CAD/CAM systems on dental ceramics and the degradation in mechanical properties after machining

The answers to these questions require the investigation of both the microstructure of the dental material in question and the machining parameters used in its shaping process. Therefore, in seeking to maximize the performance of dental restorations after machining, a balance between microstructural characteristics and machining performance must be established. However, achieving this balance is not straightforward, for it is complicated by different objectives of both the ceramics and manufacturing communities. From a ceramist's point of view, improving strength through controlling the size and orientation of grains and through the inclusion of additives in the microstructure of ceramics is an important optimization goal. Alternatively, to a machinist, the goal in machining

emphasizes the ease of material removal and quality of surface finish. These two different perspectives are sometimes contradictory. A fundamental fact is that in making a material stronger, its machinability is reduced.

But from the perspective of a dentist, it is clear that dental restorations must meet certain esthetic, physical, mechanical, and reliability requirements. Obviously, the concerns of the dentist warrant the foremost attention because they reflect the requirements of the patients. Therefore, a solution to meet the requirements of the dentist exists only if a combined effort is made by both the ceramist and the machinist. The cooperation should seek to optimize the microstructure to improve strength of dental ceramics while taking into account the conditions for better machinability.

In recent years, developments in ceramic synthesis have produced ceramic materials of varying physical and mechanical characteristics for use in restorative dentistry. One candidate material is called DICOR/MGC, a type of machinable glass ceramic (MGC). DICOR/MGC represents an improvement over existing materials because of its enhanced machinability, a result of the addition of glass in its microstructure.

In this thesis, the extent to which the microstructure of DICOR/MGC affects the machinability is investigated. Three types of DICOR/MGC are examined, namely the fine, medium, and coarse grades. The overall goal is to determine whether and how microstructure or machining parameters, or both as the case may be, contribute to degradation of mechanical properties of dental ceramics. Implications of this study to current research in dental restorations are immediately

clear because the connection of microstructure to machining performance combines the optimization concerns of material properties and machinability. As advanced manufacturing technology continues to improve CAD/CAM systems, the efficiency in fabrication of dental restorations can be further maximized, but only if the inherent physical and mechanical characteristics of such materials are likewise improved.

### **1.3 SCOPE OF THE THESIS**

The objective of this research is to perform machining of dental ceramics through the end milling process in an effort to understand their machining performance. Because CAD/CAM systems are relied on for faster and more reliable fabrication of all-ceramic restorations, understanding the machining performance of dental ceramics is of great interest to dentists. The machining performance is defined in terms of surface integrity, force measurement, and fracture toughness evaluation. This work focuses on new machinable ceramics and investigates their viability as dental restorative materials. Following is a list of the work performed in carrying out the investigation:

1. A dynamometer was designed and fabricated to serve two purposes. The first purpose is to measure the dynamic cutting force during machining. The measurement of the cutting force gives insight into the machinability of a material and serve as an on-line monitoring of the machining process. Particularly useful of the on-line monitoring effort is the indication of the machinability a material in terms of the cutting force, which can indicate the severity of the cutting conditions. Furthermore, the analysis of the cutting

force provides an understanding of the mechanism of material removal by yielding information on the chip-forming process. The second purpose is to provide a flexible platform for machining a variety of dental ceramics. Due to variation in shapes and sizes of ceramic specimens and to the need to fit to a 3-axis milling machine, a dynamometer incorporating a flexible fixture system was designed and fabricated. The construction effort is performed starting from a CAD design to machining and assembly of all components at the Advanced Design and Manufacturing Lab.

2. Experiments in machining by end milling were conducted using a systematic approach called factorial design of experiments. Such a design allows the study of the effects of machining parameters on surface integrity, force generation, and fracture toughness. Moreover, empirical expressions of these effects, in terms of the machining conditions, can be developed to provide comprehensive knowledge the machining performance. A microstructure study was also carried out to understand how the microstructure of DICOR/MGC affects the machining performance. Methods of surface preparation, including polishing, ultrasonic cleaning, and etching were performed to expose the fine and coarse microstructures of the ceramic material under investigation.
3. Experimental data on DICOR/MGC was obtained, including the cutting force, the quality of surface integrity, and the fracture strength. The machining performance of the dental ceramic material is assessed in terms of these three aspects. For the cutting force data, a data acquisition (DAQ) system was developed, incorporating the dynamometer, a DAQ software, and a computer.

For the surface integrity data, high-magnification micrographs were obtained, using an environmental scanning electron microscope (ESEM), which revealed surface and sub-surface damages during the machining process. For the fracture strength data, four-point bending tests were conducted on non-machined and machined DICOR/MGC to determine trends in strength degradation.

Thus, a comprehensive evaluation of machining performance is presented. Efforts of the work contribute to the overall goal of optimizing machining performance. A particularly important emphasis of this work is whether DICOR/MGC is a viable alternative to current material systems in use.

#### **1.4 ORGANIZATION OF THE THESIS**

The thesis is organized into seven chapters. Chapter 2 presents a literature review on traditional and advanced ceramics, the machining of ceramics, and a definition of machinability as used in this thesis. Included also is an introduction to dental glass ceramics and the use of end milling as a machining method. Chapter 3 presents an architecture for optimizing machining performance. It outlines the overall systems approach used in this thesis. Chapter 4 presents work on the microstructure of the dental ceramic material. Chapter 5 presents a design and fabrication of a dynamometer, including the data acquisition system that was developed to measure the cutting force. Chapter 6 details the experimental procedures, the designs of experiments to study the microstructure and machining of dental ceramics, and the discussion of results. Lastly, chapter 7 concludes with the thesis findings, recommendations, and suggestions for future work.

## **Chapter 2**

### **Literature Review**

In current manufacturing practices, the shaping of ceramic components to meet required specifications is performed mainly by the grinding process. The inherent brittleness of ceramics imposes such a restriction due to the formation of micro-scale cracks on and/or beneath the machined surface. In recent years, however, innovations in material processing technology have yielded new types of ceramics which have eased the concerns on brittleness. As a result, ceramic materials are capable of being machined more aggressively without concerns of weakening their inherent high strength. To understand the implications of these recent advances in ceramics and, hence, the direction of this thesis, a review of current ceramics research and application is in order. In this chapter, a literature review is presented, covering the following: traditional and advanced ceramics, conventional methods of ceramic machining, dental ceramics, CAD/CAM for dental restorations, and a definition of machinability as used in this thesis.

#### **2.1 TRADITIONAL AND ADVANCED CERAMICS**

Ceramics are generally grouped into two types, traditional and advanced. The distinction between the two groups is based on whether the raw materials are naturally occurring or man-made. Traditional ceramics are formed or sintered from naturally occurring raw materials. Examples of traditional ceramics include refractories, whiteware, cement, structural clay materials, and abrasives. Among these, refractories are used as thermally insulated structures in high-temperature

furnaces; whiteware is more commonly recognized as porcelain, electrical insulators, and dishes; structural clay materials are used as construction bricks and tiles; and abrasives include silicon carbide and aluminum oxide, which are widely used in making grinding wheels.

Advanced ceramics, on the other hand, are created from artificial combinations of metals and non-metals. Such combinations offer the engineering of many performance advantages into a ceramic material. Hence, an advanced ceramic can be customized to specific applications. As a result, advanced ceramics have greater functions, better properties, and wider applications. Table 2-1 lists a variety of functions made possible by advanced ceramics, including their properties and applications [Musikant, 1991].

Table 2-1. Advanced ceramic functions, properties, and applications

| <b>FUNCTION</b>       | <b>PROPERTIES</b>  | <b>APPLICATIONS</b>  |
|-----------------------|--|--|
| Thermal               | Refractories, insulation, heat collection, thermal conductivity                | Heat sink, electrode material, high-temperature furnace lining                 |
| Mechanical            | High strength, wear resistance, low thermal expansion, lubrication             | Tools & jigs, abrasives, turbine blades, solid lubricants                      |
| Biological & Chemical | Bio-compatibility, catalysis adsorption, corrosion resistance                  | Artificial bone & tooth, heat exchanger, chemical equipment                    |
| Electrical & Magnetic | Electrical insulation, conductivity, semiconductivity, piezoelectric, magnetic | Integrated circuit substrate, resistance heating element, piezoelectric filter |
| Optical               | Optical condensing, fluorescence, translucence, optical conductivity           | Optical communication cable, laser diode                                       |
| Nuclear               | Radiation resistance, refractoriness, high-temperature strength                | Nuclear fuel, control material, reactor mining                                 |

In restorative dentistry, a material to be used must have appropriate mechanical, biological, chemical, and optical properties to function in the oral environment. Advanced ceramics, with their varied and wide-ranging capabilities, are ideally suited for the task since they closely match the esthetics and mechanical properties of real teeth. The major drawback of ceramics is, of course, their brittle behavior under loading. As discussed next, this brittleness leads to machining difficulty which must be overcome if mass production of ceramic parts is to become economically feasible.

## **2.2 MACHINING OF CERAMICS**

Although ceramics offer enormous functional benefits, machining remains a challenging job because the presence of micro-cracks induced from the brittleness. Various methods, such as grinding, honing, lapping, and polishing, are developed and used to machine brittle materials, but all are based on geometrically undefined cutting edges such that material removal rates and shaping capabilities are severely limited. Additional disadvantages associated with these methods include the use of expensive super abrasives, high tool wear, and high machining force [Konig, 1991].

Yet, lapping and polishing are capable of yielding remarkable surface finish and reduced sub-surface damage. One current theory behind these fine-scale machining processes suggests the existence of critically small material removal rates in which ductile-regime machining is possible. The theory implies that a physical transition is made during the machining operation from a system of brittle fracture to one of plastic flow if a critical depth of cut model is applied [Bifano, 1992]:



$$d_c \propto \left( \frac{E}{H} \right) \left( \frac{K_c}{H} \right)^2 \quad 2-1$$

In equation 2-1,  $d_c$  is the critical depth of cut that defines the transition from plastic to brittle behavior,  $E$  is the elastic stiffness,  $H$  is hardness representing the plastic deformation resistance, and  $K_c$  is the fracture toughness of the brittle material. Application of this model suggests the existence of a brittle-ductile transition based on the percentage of surface fracture as a function of grinding infeed rate.

Further evidence of the existence of plastic deformation in the grinding of ceramic materials is presented in the work of Subramanian and Ramanath, 1992. Their research suggests that the mechanism of material removal during precision grinding combines both brittle fracture and plastic deformation. Furthermore, the ratio of plastic deformation to brittle fracture may be increased by controlling the parameters of machining and machine tool. Figure 2-1 illustrates the variables that determine the material removal process [Subramanian, 1992].





| Material Removal Mechanism | Plastic Deformation   | Brittle Fracture  |
|----------------------------|---|---|
| Grit Size                  |  |  |
| Material Removal Rate      | Low   | High  |
| Force/Grit                 | Small   | Large   |
| Chip Thickness             | Small   | Large   |
| Surface Finish             |  |  |
| Part Strength              | High  | Low   |

Figure 2-1. Dependence of material removal mechanism on machining conditions

Although milling is one of the traditional methods of machining metals, it is however being explored as an alternative machining method to abrasive machining with the introduction of glass machinable ceramics. Like all machining methods, milling has its advantages and disadvantages. Of the positives, milling offers large material removal rates under a controlled environment; the cutting parameters of spindle speed, feed rate, and depth of cut are set to pre-determined levels. However, on a negative note, the milling process produces significant surface and sub-surface damage in ceramics. The material removal mechanism of crack initiation leading to brittle fracture in ceramics is difficult to control. To further illustrate this, milling can be characterized by a five-stage process, as depicted in Figure 2-2 [Satish, 1993].

In stage 1, a cutting tool impacts an edge of the ceramic part and induces a stress field in the material, as indicated by the contour lines of constant stress. The tool represents a flute of an end mill as it rotates into the ceramic material, while the dashed line indicates the depth of cut. Note that different stress fields can be induced as the angle, i.e. rake angle, of the tool is changed.

In stage 2, as the tool continues cutting into the material, strain and stress develops and intensifies locally at grain boundaries. The stress field becomes concentrated at these boundaries, an indication that the stress is rapidly approaching its yield strength limit. Since in ceramics the material failure is governed by brittle fracture, when the stress approaches the yield strength, it also approaches its ultimate strength. In this case, the concentration of stress at the grain boundaries overcomes the fracture strength of the material, thereby giving rise to local crack initiation.

In stage 3, with more loading by the tool, the cracks in stage 2 grow and propagate mainly along the grain boundaries where other stress concentration sites have been developing. As shown in Figure 2-2, the cracking phenomenon is not just limited to material above the depth of cut, but it is also expanding below the line.

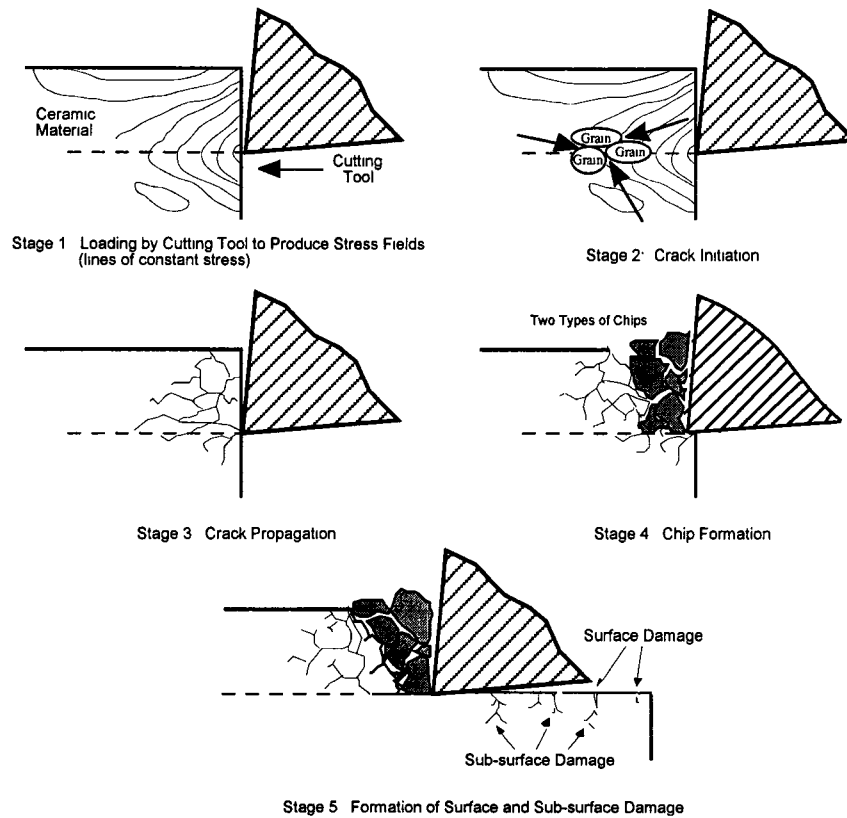


Figure 2-2. A five-stage process in the material removal mechanism of ceramics

In stage 4, the crack propagation of stage 3 has progressed far enough to connect with other stress concentration sites. Once connections are made with other cracks, the result is the formation of distinct, whole volumes of material called chips which are now completely free from the ceramic material. From this, two types of chips can be identified, as shown in Figure 2-3. One type is formed on



(a) Formed from chip-tool interface



(b) Formed in front of the cutting tool

Figure 2-3. Two types of chips observed in the machining of ceramics

the chip-tool interface in the secondary cutting zone due to the presence of high temperature on the interface, which is defined as the region between the rake face of the tool and the ceramic material where high shearing takes place. The other type of chips is formed in front of the tool by the mechanism of cracking leading to brittle fracture and chipping.

Finally, in stage 5, the chipping from stage 4 results in a machined surface which is scarred by surface and sub-surface cracks. As this stage clearly shows, control of the surface and sub-surface damage is critical to ensuring reliable performance of the machined part during service life. Because the ceramic material is already inherently brittle, such damage, if uncontrolled, could lead to faster catastrophic failure.

The five-stage process in the mechanism of material removal discussed above implies that the machining-induced damages could be controlled by varying the cutting conditions, e.g. the depth of cut. In this thesis work, the machining is performed using a computer numerical control (CNC) milling machine that allows for very precise control of the three machining parameters, namely spindle speed, feed rate, and depth of cut. Figure 2-4 shows an end mill tool during a cutting operation. Note in the illustration that the cutter has two flutes, or teeth, the same number used for the cutting tool in this thesis work. Figure 2-4 also defines the three key machining parameters for the end milling process.

During machining, the teeth act as single-point cutters with trajectories that are described by a trochoid path [Ismail, 1993]. Note also that the cutting is contributed by the helical sharp edges as well. In a perfectly plastic material, the

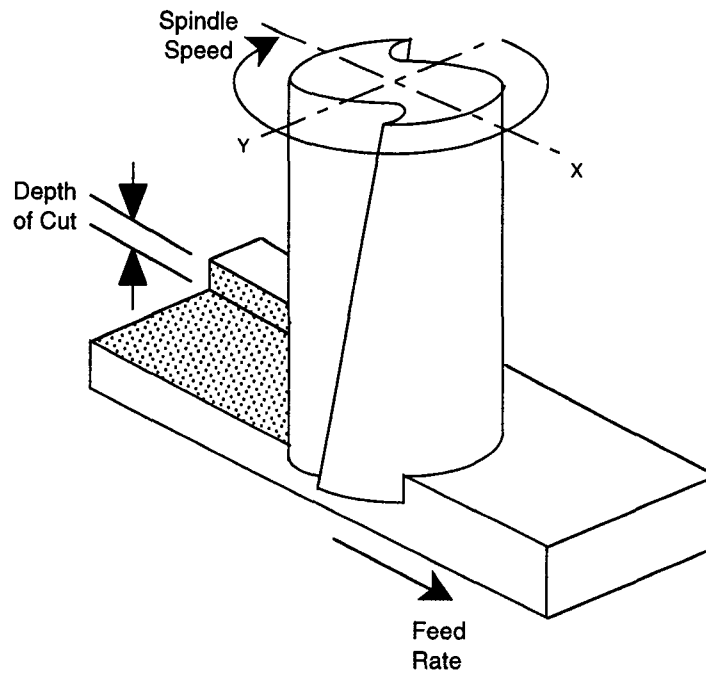


Figure 2-4. An end milling operation defined by three parameters

surfaces produced by an end mill tool would show plastic deformation, but for brittle materials, the surfaces and especially the edges are characterized by severe chipping due to cracking.

From this discussion, it is clear that the brittle behavior of ceramics must be controlled to ensure quality in machining performance. With advances in ceramics research, material scientists are able to control the microstructure to yield the desirable mechanical properties. With machinable ceramics, significant reductions in surface and sub-surface cracking during machining can be achieved, resulting in better part geometry and surface integrity. Thus, the milling of ceramics represents a new approach to shaping ceramics based on improvements in material properties.

## 2.3 DENTAL GLASS CERAMICS

The use of a dental ceramic is based on several factors, including esthetics, strength, fit, biocompatibility, cost, and ease of fabrication. Unfortunately, not a single material exists that matches all of the above characteristics satisfactorily. Therefore, several types of dental ceramics are available and used depending on particular applications. Figure 2-5 shows the variety of materials that exist to the dentist [Giordano, 1996]. As shown in the figure, there are two systems available in restorative dentistry. The first is a porcelain-fused-to-metal system. In this system, a ceramic is bonded to a metal to provide strength since the ceramic is quite weak. This system is by far the most used in restorative dentistry, accounting for 80% of all restorations. The second is an all-ceramic system in which the restoration is entirely made of ceramic. The advantage of an all-ceramic system is that the esthetics of natural teeth are better matched. However, depending on the application, fracture strength is sometimes a concern in an all-ceramic system since, as Figure 2-6 shows, some systems are better than others [Giordano, 1996].

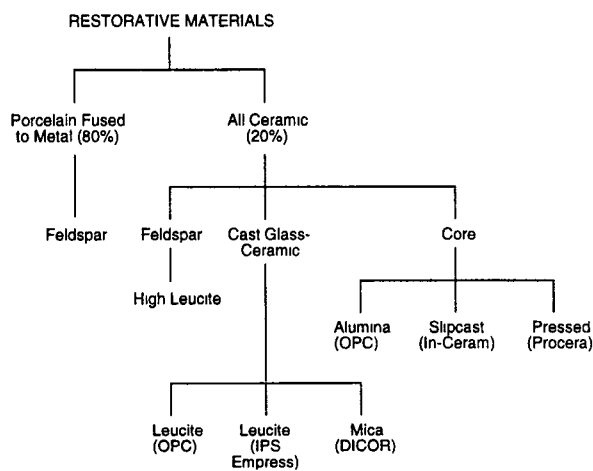


Figure 2-5. Dental ceramic materials for restorations

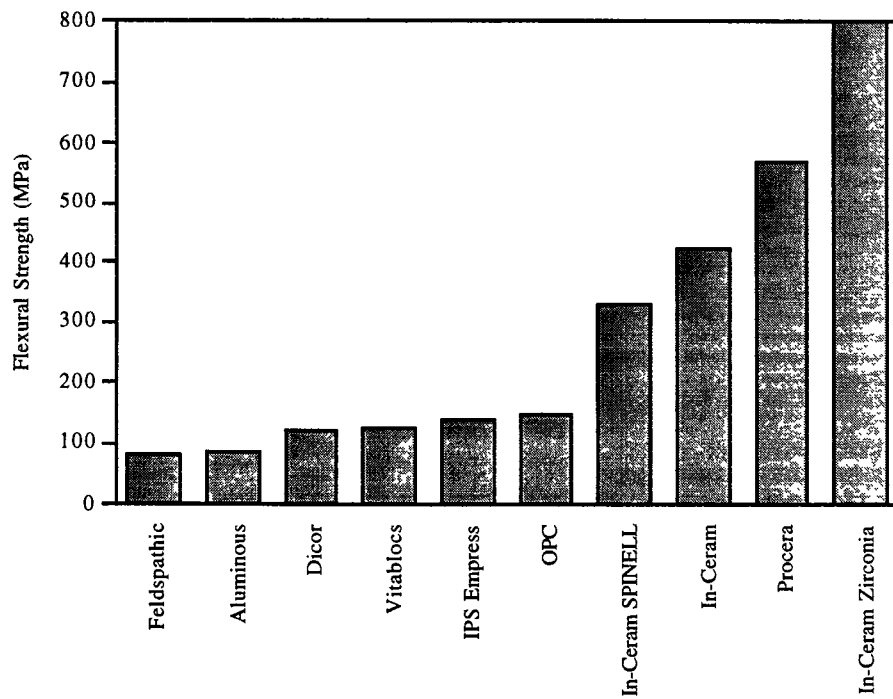


Figure 2-6. Comparison of fracture strengths of existing dental ceramics

Figure 2-6 also illustrates the previous discussion regarding the issue of balance of microstructural properties and machinability when choosing a dental ceramic material for restoration. For example, the four materials, In-Ceram Spinell, In-Ceram, Procera, and In-Ceram Zirconia, to the right of Figure 2-6 all have high values of fracture strength, which, in itself, is a good material characteristic. However, such high strength makes for very difficult machining, resulting in high cutting forces and extensive cracking. Therefore, in picking a dental ceramic material, a compromise on material property and machinability must be established.

In this thesis, the investigation of machining performance of dental ceramics is focused on an all-ceramic system. One such sub-system is



DICOR/MGC, a machinable glass ceramic (MGC) developed at Corning Glass Works [Grossman, 1973]. The chemical makeup of DICOR/MGC consists of  $\text{SiO}_2$ ,  $\text{K}_2\text{O}$ ,  $\text{MgO}$ ,  $\text{Al}_2\text{O}_3$ , and  $\text{ZnO}_2$ . During the heat treatment process, micaceous crystals form to give DICOR its strength and machinability. This crystalline phase is composed of tetrasilicic fluoromica,  $\text{K}_2\text{Mg}_5\text{Si}_8\text{O}_{20}\text{F}_4$ , and makes up about 50% of the ceramic [Giordano, 1996]. These crystals, or mica flakes, are elongated, cylindrical grains which vary in platelet sizes from 1  $\mu\text{m}$  to 10  $\mu\text{m}$ , depending on the heat treatment temperature. For example, at a treatment temperature of 1000  $^\circ\text{C}$ , the DICOR that results is called "fine" and contains mica platelets of 1.1  $\mu\text{m}$  in size. Its fracture strength ranges from 240 to 280 MPa. Table 2-2 lists the three types of DICOR/MGC manufactured from different heat treatment temperatures [NIST, 1996].

Table 2-2. Some mechanical properties of DICOR/MGC

| Nomenclature | Heat Treatment Temperature ( $^\circ\text{C}$ ) | Mica Platelet Size ( $\mu\text{m}$ ) | Fracture Strength (MPa) |
|--------------|---|--------------------------------------|-------------------------|
| Fine         | 1000  | 1.1                                  | 240-280                 |
| Medium       | 1060  | 3.7                                  | 210-245                 |
| Coarse       | 1120  | 10.0                                 | 115-175                 |

## 2.4 MACHINABILITY

In the machining community, the definition of machinability is an elusive concept. That is because there is no general agreement on how the term should be defined exactly. For example, one definition of machinability associates some aspects of the cutting process, such as the tool life, tool wear rate, energy required for a standard rate of material removal, or surface finish. Another definition uses

general concepts, such as the "totality of all the properties of a work material which affect the cutting process," and "the relative ease of producing satisfactory products by chip-forming methods [Smith, 1989]."

While an agreement on a standard definition may be difficult to reach, a number of machinability tests does exist currently. In general, machinability tests are categorized by four types: machining, non-machining, ranking, and absolute [Mills and Redford, 1983]. In the machining tests, machinability of a material is determined through some turning operations in which the effects of the workpiece, tool, or cutting fluid, or combinations of the three parameters, are examined. This is in contrast to the non-machining tests, where chemical, microstructural, or physical properties are determined. Machinability tests may also be classified by either ranking or absolute. In ranking, machinability of a material is determined relatively to other materials which have been machined under the same cutting conditions. On the other hand, in an absolute test, machinability is determined by a range of cutting conditions. Obviously, the absolute test is superior to the ranking because it provides a comprehensive picture of the machining characteristics of a type of material. However, the absolute test is time-consuming. For that reason, short-term machinability tests have been developed. Table 2-3 lists twelve such tests, by type and test parameter.

In this thesis, the machinability of dental ceramics is investigated. However, it is limited in the following manner: for reasons of simplicity and practicality, this thesis defines machinability of dental ceramics in terms of 1) the force generated during machining, 2) the quality of surface integrity formed after machining, and 3) the degradation of fracture strength after machining.

Table 2-3. Types of short-term machinability tests

| Test                    | Type      |               |          |         | Test Parameter |      |               |
|-------------------------|-----------|---------------|----------|---------|----------------|------|---------------|
|                         | Machining | Non-machining | Absolute | Ranking | Workpiece      | Tool | Cutting Fluid |
| Chemical Composition    |           |               |          |         |                |      |               |
| Microstructure          |           |               |          |         |                |      |               |
| Physical Properties     |           |               |          |         |                |      |               |
| Rapid Facing            |           |               |          |         |                |      |               |
| Constant Pressure       |           |               |          |         |                |      |               |
| Taper Turning           |           |               |          |         |                |      |               |
| Variable-Rate Machining |           |               |          |         |                |      |               |
| Step Turning            |           |               |          |         |                |      |               |
| Degraded Tool           |           |               |          |         |                |      |               |
| Accelerated Wear        |           |               |          |         |                |      |               |
| Tapping                 |           |               |          |         |                |      |               |
| HSS Tool Wear Rate      |           |               |          |         |                |      |               |

The force measurement is an important indicator of machinability for it provides instantaneous feedback during the cutting process. Likewise, the surface finish shows the extent to which a material retains its geometric and dimensional integrity. Lastly, the degradation in fracture strength after machining is vital to determining the performance reliability of a material during service.

## 2.5 CERAMIC MICROSTRUCTURES

While the issue of machinability as a measurement of machining performance remains clouded, the underlying factor affecting machinability is, however, well understood. This is because every property of a ceramic, from strength to hardness to machinability, is a function of its microstructure [Loehman, 1993]. This importance of microstructure on defining physical properties of a ceramic may be further examined by noting the various features.

The first feature is the grain size and shape which have important implications in the machining performance of ceramics. Since the material removal mechanism in ceramics starts from micro-scale cracks and ends with brittle fracture, by controlling the grain geometry in the microstructure, the crack propagation can be arrested or made to travel through a tortuous path. The particular path that a crack takes can be either transgranular, i.e. through the grain, or intergranular by way of the grain boundaries. In such a case as intergranular cracking, the mechanism of grain-pullout results when the cracking propagates completely around a whole grain and dislodges it. In light of such cracking phenomena, small, irregularly shaped grains may yield stronger ceramics, while larger grains may produce weaker ones. In terms of machinability, then, it is critical that the grain geometry be controlled appropriately. Figure 2-7 shows a schematic of the microstructural features in ceramics.

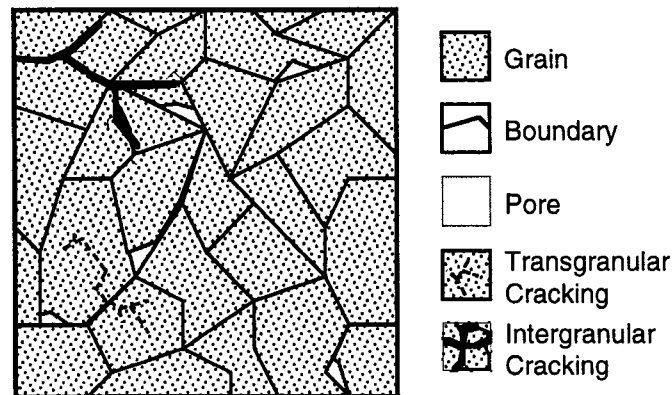


Figure 2-7. Ceramic microstructural features

The second microstructural feature which contributes to the machinability is porosity. Porosity of ceramics affects machinability because pores in ceramics lead to stress concentrations where micro-scale cracks can developed. In Figure 2-7, the

pores are represented by the small shaded regions. Note that pores occur between grains, and that they are inherent features in ceramics because they are mostly unavoidable due to the processes used in making ceramics, such as sintering of ceramic powders. Because of sintering, full density is often difficult to achieve without applying pressure during firing.

Other microstructural features related to machinability include: multi-phases and volume fraction. Consequently, the microstructure of ceramics is often more complex than the one shown in Figure 2-6, with different phases present within the material. The co-existence of different phases, like the pores, affect the crack propagation, and hence machinability, because the path of propagation is no longer homogeneous. The different phases mean that the transfer of strain energy is discontinuous as the cracking moves through the phases, which has the effect of arresting the propagation. Thus, the study of the secondary phases on the grain boundaries is a basic requirement to understand the machinability of a material. Meanwhile, the use of volume fraction satisfies the requirement of machinability by measuring the relative quantities of the various phases in the microstructure. The volume fraction is obtained by examining high-magnification micrographs, typically from a scanning electron microscope, and counting the proportion of the interested phase or feature within the micrograph.

## Chapter 3

### Architecture for the Optimizing of Machining Performance

In this thesis research, an architecture is proposed concerning the optimization of the machining performance of DICOR/MGC. The architecture consists of four parts, as outlined in Figure 3-1. They are characterization of microstructure, identification of machining parameters, on-line monitoring of the machining operations, and evaluation of machining performance.

The first task in this optimization architecture is the characterization of microstructural features in DICOR/MGC. This work lays the foundation for machining experiments because the fact is that microstructure and machining are intimately related. The second task is the identification of machining parameters.

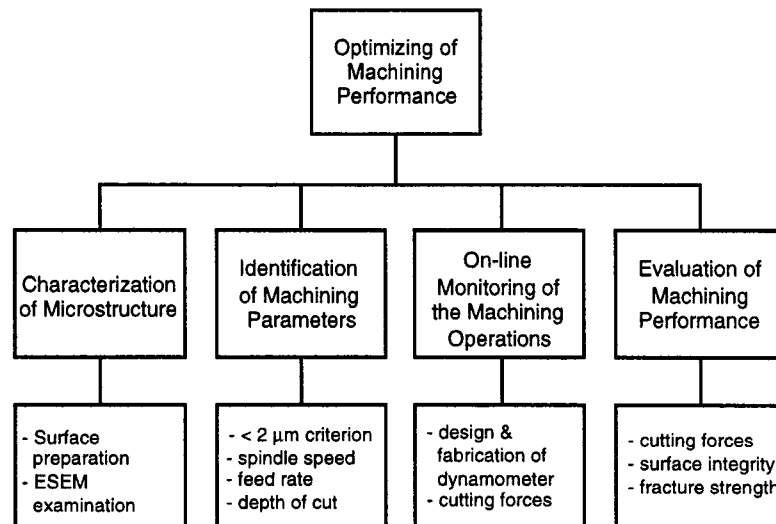


Figure 3-1. Flowchart of the optimization architecture

### 3.1 CHARACTERIZATION OF MICROSTRUCTURE

The microstructure of ceramics plays a crucial role in determining the material behavior during machining. The microstructure affects such properties as strength, mechanism of failure, and physical appearance. In this thesis, the effects of microstructure on machining performance of DICOR/MGC are explored by conducting machining and strength experiments on three grades of the DICOR/MGC material. The three grades have different microstructural characteristics due to features formed during material synthesis. These features have important implications on machining performance.

For the first grade, the DICOR/MGC is referred to as "fine," or DICOR/MGC-fine. As the name suggests, the microstructure of DICOR/MGC-fine is composed of small grains. For the second grade and third grade, the DICOR/MGC is referred to as "medium", or DICOR/MGC-medium, and "coarse", or DICOR/MGC-coarse, respectively. Clearly, the medium and coarse materials have corresponding grain sizes, as the names suggest. Aside from the differences in grain sizes, the three materials are fundamentally the same in terms of chemical composition. All three DICOR/MGC materials incorporate single mica crystals within a glass matrix. It is the presence of the glass that provides a conducive material structure for machining.

In terms of optimization of machining performance, the study of the microstructure of DICOR/MGC is the first appropriate step. By understanding the contribution of microstructures on material behavior, the identification of appropriate dental materials for restorations is greatly facilitated. Moreover,

knowledge of what types of microstructural features are present, and how they can be benefit or hinder performance are key to addressing issues of optimization.

### **3.2 IDENTIFICATION OF MACHINING PARAMETERS**

The second part of the optimization architecture is the identification of machining parameters. The identification entails correlating the machining performance with the three machining parameters of spindle speed, feed rate, and depth of cut. Using factorial design of experimentation, these parameters are empirically related to the cutting forces and flexural strength measurements in the forms of mathematical expressions. The expressions predict the machining performance within the range of the high and low settings used by the factorial design.

As illustrated in the schematic in Figure 3-2, the machining parameters have great influence on machining performance. For example, regarding the cutting process, the machining parameters not only control the shaping process, but also influence the mechanism of material removal. Furthermore, the influence of the machining parameters extend to the quality of surface finish, as indicated by the surface roughness in Figure 3-2, and to the subsequent generation of cutting forces as well. The quality of surface finish is an extremely important aspect of machining performance optimization because, due to the harsh and cyclic loading environment of the mouth, ceramic restorations may fail due to growth in micro-cracks left from the machining operation.



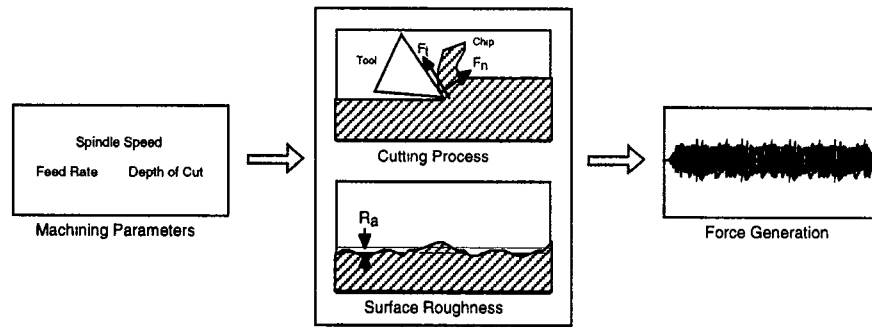


Figure 3-2. Contribution of the machining parameters to the cutting process, surface roughness, and force generation

### 3.3 ON-LINE MONITORING OF THE MACHINING OPERATIONS

The third part of the optimization architecture involves the on-line monitoring and measurement of the dynamic cutting force during machining. The objective in this effort is to gain insight into the generation of forces during machining, to correlate the force measurement to machining parameters, and to assess the interaction of force measurement with fracture strength degradation.

To make possible the on-line monitoring and measurement of the cutting force, a dynamometer is designed and fabricated. The major components of the dynamometer include the sensing element, the component that detects the strain induced on the dynamometer by the cutting force and the vise-fixture component for mounting machining specimens to the dynamometer. Some technical issues regarding the functional design of the dynamometer include the sensitivity of the signal response and the rigidity of the dynamometer structure. The challenge is to strike a balance between sensitivity and the rigidity. If a dynamometer is too sensitive, it loses its rigidity; likewise, if it is too rigid, it loses its sensitivity. In both cases, accuracy is lost too.

### 3.4 EVALUATION OF MACHINING PERFORMANCE

The fourth and last part of the optimization architecture is the evaluation of machining performance, which entails analyzing the cutting force and the fracture strength of machined DICOR/MGC and relating the results to the its unique microstructural features. The components of the evaluation of the machining performance are shown in Figure 3-3. Hence, the components of microstructural analysis, cutting force measurement, and fracture strength evaluation are unified.

The evaluation of machining performance is based on a factorial design of experimentation. In particular, the design allows for systematic analysis of the experimental data, including empirical models that express the quantitative relationships of the three key machining parameters to the feed and transverse cutting forces, and to the fracture strength. From these empirical models, optimization of machining performance is established.

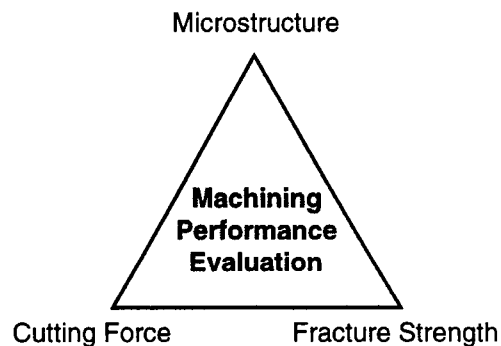


Figure 3-3. Components of the evaluation of machining performance

## **Chapter 4**

# **Characterization of the Microstructure of Dental Ceramics**

In this chapter, the characterization of the microstructures of DICOR/MGC is presented, with the purpose being to understand the connection between microstructural features and machinability. The experimental investigation consists of a systematic examination of the microstructures of the three types of DICOR/MGC, namely, fine, medium, and coarse. The investigation relies on examination of high magnification micrographs obtained from an ESEM/computer-based system.

### **4.1 EXPERIMENTAL METHODOLOGY**

In this investigation, the microstructures of DICOR/MGC are analyzed as described by the procedures in Figure 4-1. To begin, the three types of DICOR/MGC are prepared in two formats: raw, i.e. no modification is done to the stock material, and polished. The raw format is used to serve as a base line for comparison in the investigation. On the other hand, polishing, is used to prepare the specimens. Polishing has been a standard practice to reduce the variation in microstructural analysis.

Typically, a surface is polished with very fine particles, usually diamond paste whose particles are of micron size. The polishing removes debris, loose particles, and rough surfaces on the material. Once the polishing is completed and the surface finish is acceptable based on some predetermined criteria, cleaning of the

specimens is performed using an ultrasonic cleaner to remove dirt, oil, and other types of debris from the prepared surfaces. The principle behind the ultrasonic cleaner is that it uses high frequency sound waves to loosen and remove debris on the surface of a material which is submerged under water. The procedure is assisted with the addition of cleaning agents mixed into the water. Visually, the setup does not give any indication of cleaning activity, but this is only because of the high frequency used.

In the next step, etching is applied to each material to remove the smear layer left behind from the polishing. For materials such as the DICOR/MGC, etching also removes the glassy phase, making the task of exposing the features of the micaceous crystals easier. Finally, the cleaned and etched specimens are put into an ESEM for examination.

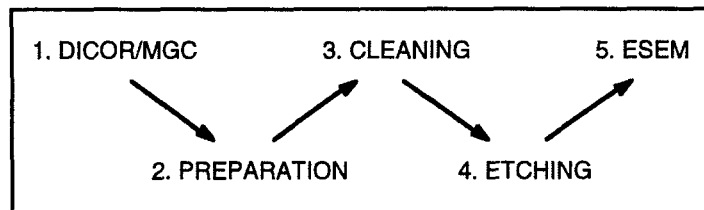


Figure 4-1. Procedure for analyzing microstructures

It should be noted here that the etching is very critical to obtain good micrographs of the microstructures. In general, the etching process is quite simple, but the duration of the processing time varies depending on the material used. Etching is done by applying a 10% by weight solution of Ammonium Bifluoride to the surface of a sample. After the predetermined etching time has passed, the etching process is halted by submerging the DICOR/MGC materials in a water bath

for about 30 seconds. The sample is cleaned with acetone as a final step in the process. The 10% by weight solution of Sodium Bifluoride attacks the grain boundaries and exposes the microstructure of DICOR/MGC.

## 4.2 ESEM-COMPUTER-BASED SYSTEM

In order to obtain images for microstructural analysis, a special, high-magnification microscope is used, called an environmental scanning electron microscope (ESEM). The microscope is part of a computerized image processing system, shown in Figure 4-2 [Zhang, 1996]. As illustrated, the process begins with a prepared specimen, either raw (non-polished), or polished. The specimens are 28 mm long bars with rectangular cross-section measured as 6 mm wide and 4 mm high x 28 mm. The specimen is placed into the ESEM where microstructural images at magnification of 2500x can be clearly observed. The captured images of 640 pixels x 640 pixels are saved in a digital format, stored in the computer system, and can be retrieved for microstructural analyses.

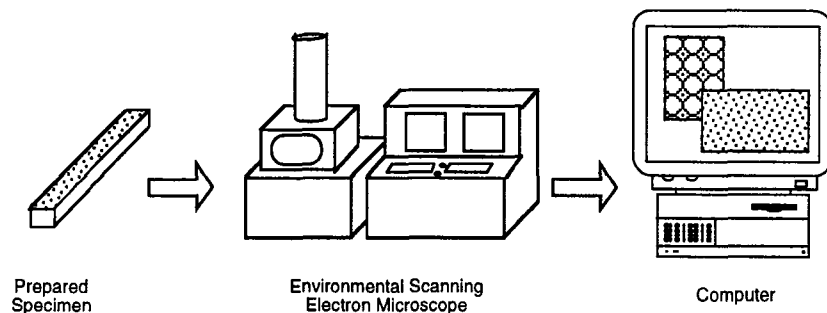


Figure 4-2. ESEM/Computer-based system for microstructural analysis

In this system, the use of an environmental scanning electron microscope is necessary because ceramics are electrically non-conductive materials. For that reason, a regular SEM would be incapable of viewing the ceramics. The environmental SEM, on the other hand, employs an inert gas in the specimen chamber to scatter electrons generated from a gun into a material. Any electron reflected back or given off by the material is collected by the microscope and an image is formed on the screen. Thus, the use of the ESEM is ideal for bio-materials.

### **4.3 MICROSTRUCTURAL ANALYSIS**

Microstructure plays a significant role in governing the machining behavior of ceramics, in terms of its susceptibility to machining-induced surface and subsurface cracking. Therefore, a clear understanding of the microstructural aspect of each material, such as the grain size, orientation, and boundary relations are necessary to interpret machining results.

Figure 4-3 presents SEM micrographs obtained from the performed microstructural analyses. The two columns represent the information before and after machining. The three rows represent the three types of microstructural characteristics, namely, DICOR/MGC-Fine, DICOR/MGC-Medium, and DICOR/MGC-coarse materials, respectively. As shown in Figure 4-3, the polished specimens produce better results than those of the non-polished specimen in terms of grain size, grain shape and grain boundaries. For example, the grains of the DICOR material are characterized by elongated rod-like structures of varying sizes, depending on whether the material is fine, medium, or coarse. As expected, the

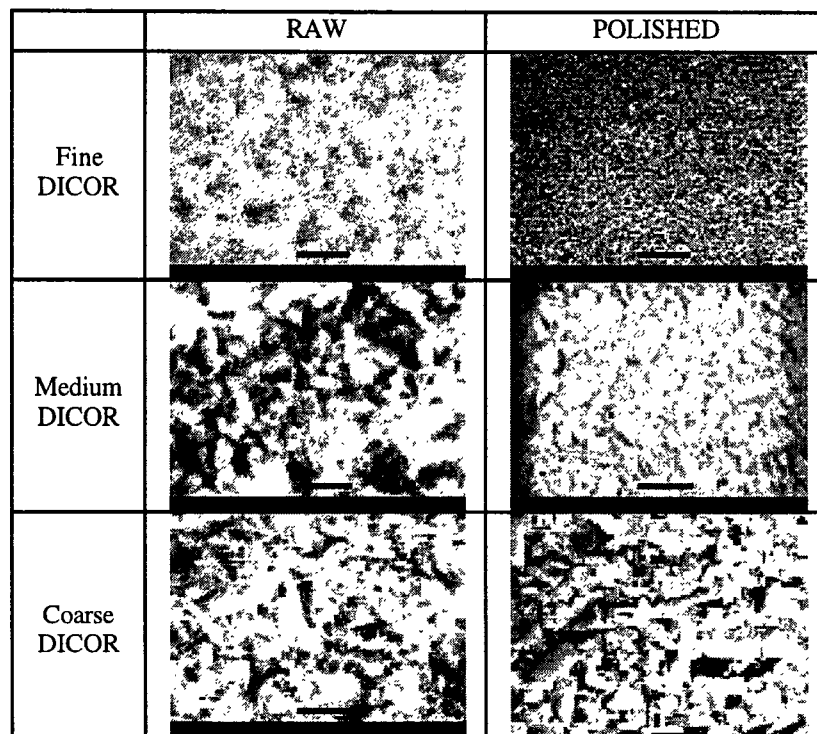

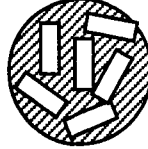
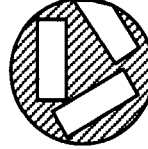


Figure 4-3. Microstructures of Dental Ceramics

micrographs show that fine and coarse DICOR contain the smallest and largest grains, respectively, while the medium DICOR is somewhere in between. The visual evidence also reveals that these grains are suspended in a glassy phase, as shown most dramatically by the medium DICOR micrograph under the "polished" column in Figure 4-3. Thus, for DICOR, its microstructural features are characterized by grains of similar shapes but of different sizes, and by the existence of a two-phase structure. Table 4-1 is a summary of the microstructural characteristics observed for the DICOR/MGC-Fine, DICOR/MGC-Medium, and DICOR/MGC-coarse materials.

Table 4-1. Microstructural features of DICOR/MGC

| DICOR/MGC   |   |  |
|---|---|--|
| Fine  | Medium  | Coarse   |
| Small sized elongated rod-like grains embedded in a glassy phase                    | Medium sized elongated rod-like grains embedded in a glassy phase                   | Large sized elongated rod-like grains embedded in a glassy phase                     |
|  |  |  |



## **Chapter 5**

### **Design and Fabrication of a Dynamometer**

The goal of constructing a dynamometer is to carry out in-process measurements of the cutting force produced during machining. In machining science, the cutting force is an important performance index because it has a direct relation with the settings of machining parameters, material properties and the material removal mechanism(s). Because the cutting forces provide a deep insight into the mechanical behavior of a material during material removal, the machining performance of the DICOR/MGC materials may be assessed from the information obtained from measuring the cutting force generated during the machining of DICOR/MGC. Therefore, design and fabrication of the dynamometer represents a crucial part of this thesis work. In the discussion to follow, a strain gage-based dynamometer, a data acquisition (DAQ) system, and system calibration are presented.

#### **5.1 STRAIN GAGES**

A dynamometer is a device that measures forces. There are several sensing devices which are capable of accomplishing this task. Piezoelectric sensors are widely used in dynamometers commercially available in the market. However, they are very expensive. In this research, the focus of designing a dynamometer to specifically fit the need of measuring the cutting force during the machining of DICOR/MGC is using strain gages. These strain gages are mounted on the sensing part of the dynamometer to detect changes in electrical resistances as the cutting

force is being applied to the dynamometer. Note that the cutting force is characterized by a spatial vector. Identification of such a spatial vector calls for the detection of its three components. The concept adopted in this research is to measure the three cutting force components in the feed, transverse, and normal directions. After the measurements, manipulation of a vectorial sum is performed to determine the magnitude and orientation of the cutting force by the following formulas:

$$F = \|f_{feed}\vec{i} + f_{trans}\vec{j} + f_{norm}\vec{k}\| = \sqrt{f_{feed}^2 + f_{trans}^2 + f_{norm}^2}$$

$$\cos\alpha = \frac{f_{feed}}{F}; \cos\beta = \frac{f_{trans}}{F}; \cos\gamma = \frac{f_{norm}}{F}$$

The force measurement system is based on the following principle: the change of electrical resistances are recorded as signals and, through calibration, are converted to force signals. In general, the ability of a dynamometer to measure the force relies on the action of a strain gage to change electrical resistance when strain is induced on it by the force. How much a strain gage changes in resistance, then, is measured by the strain sensitivity factor, defined as

$$\text{Strain sensitivity factor} = \frac{\text{unit change in resistance}}{\text{unit change in length}} = \frac{\Delta R/R}{\Delta L/L}$$

Note that the denominator term, the unit change in length, is the definition of strain. For a highly sensitive strain gage, a large change in resistance corresponding to a small strain is desired. The strain sensitivity factor, called the gage factor, is critical to the accuracy of measurements. The higher of a gage factor, the better the quality of force measurements will be.

For this dynamometer design, metal foil strain gages are used to measure the strain. The gage factor is 2.135. An example of the strain gages used in this research is shown in Figure 5-1 [Measurements Group, 1989]. These foil strain gages consist of tiny metal foils which are about 0.0002 in. thick [Dally, et al., 1984 and 1993, and Murray, 1992] . When mounted onto a dynamometer, the gage

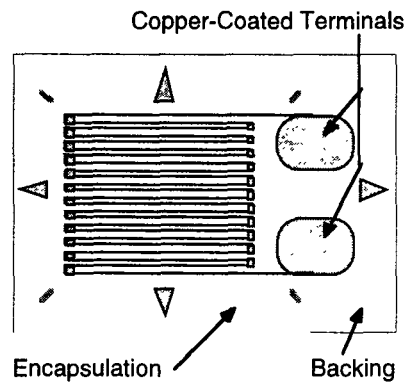


Figure 5-1. An example of a foil strain gage

is stretched or pulled depending on how the forces are applied to the dynamometer. As the length of the metal foil is distorted, its electrical resistance varies accordingly. Thus, if a gage is connected to an electrical circuit, the output of the circuit would be changed following the change of electrical resistance. In general, the changes can be measured in voltage. When a data acquisition (DAQ) system is used to digitize the output signal, the magnitude of the cutting force can be determined through signal processing.

In this thesis research, foil strain gages are used because more contact surface area per resistance volume of the metal foil element is possible than wire strain gages. In addition, because of their thinness, foil gages can accommodate

surfaces with small radius of curvature. Heat dissipation is another advantage to using foil gages because of the large contact area. Moreover, creep and hysteresis are minimized by the large contact area which reduces shearing stresses.

Finally, foil strain gages exhibit an acceptable gage factor, GF, the standard measure of the strain sensitivity in the direction of the wire axis. These gages are constructed so that the greatest sensitivity is in the direction of the wire axis, but some strain can be picked up in the transverse direction. This leads to strain errors and are due to the transverse sensitivity of the gage. Normally, the transverse strains are picked up from torsion applied to the dynamometer. Fortunately, the transverse sensitivity of a gage is small compared to the GF. In this thesis, gages with a transverse sensitivity of 0.005 ( $\pm 0.002$ ) are used.

## **5.2 WHEATSTONE BRIDGE**

The Wheatstone bridge is a special electrical circuit made up of strain gages that measures voltage changes. An example of a Wheatstone bridge is shown in Figure 5-2. This bridge is called a full bridge because it uses four strain gages as resistance elements. Other types include half and quarter bridges.

### **5.2.1 Bridge Equations**

The strain gages are represented as resistance elements  $R_1$ ,  $R_2$ ,  $R_3$ , and  $R_4$  in Figure 5-2. Normally, these gages are attached on the surfaces of a beam or cylinder which can elastically deform due to an applied force. The beam or cylinder acts, thus, as the dynamometer's sensing element. As illustrated in Figure 5-2, the bridge

is fed by a constant source of voltage. When the sensing element is perturbed slightly, the resistances of the gages are changed to produce a voltage output of  $E + \Delta E$ , where  $E$  is the output without an applied force, and  $\Delta E$  represents the slight change in voltage due to the force.

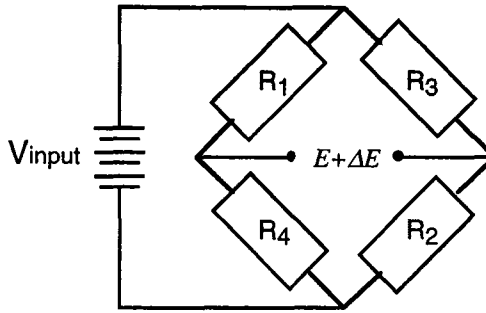


Figure 5-2. Circuit configuration of a full Wheatstone bridge

Ideally, the bridge should be balanced initially, or  $E = 0$ . For this condition to occur, the product of one opposite pair of arms (strain gages) must equal the other opposite pair, i.e.,

$$R_1 R_2 = R_3 R_4.$$

If a constant  $a$  is defined as

$$\boxed{\frac{R_1}{R_4} = \frac{R_3}{R_2} = a}$$

then the small change in voltage output,  $\Delta E$ , is given by

$$\Delta E = V_{INPUT} \frac{a}{(1+a)^2} \left[ \frac{\Delta R_3}{R_3} - \frac{\Delta R_1}{R_1} + \frac{\Delta R_4}{R_4} - \frac{\Delta R_2}{R_2} \right] (1-n) \quad 5-1$$

where  $\Delta R_{1,2,3,4}$  represent the small changes in resistance of the strain gages and  $n$  is a nonlinearity term approximated by

$$n = \frac{1}{1 + \frac{a+1}{\frac{\Delta R_2}{R_2} + a \frac{\Delta R_1}{R_1} + a \frac{\Delta R_3}{R_3} + \frac{\Delta R_4}{R_4}}} \quad 5-2$$

In reality, a full Wheatstone bridge is constructed with four strain gages having the same resistance value,  $R_g$ . Thus,  $a = 1$ , and Equations. 5-1 and 5-2 can be simplified to:

$$\Delta E = \frac{V_{INPUT}}{4} \left[ \frac{\Delta R_3 - \Delta R_1 + \Delta R_4 - \Delta R_2}{R_g} \right] (1-n) \quad 5-3$$

$$n = \frac{1}{1 + \frac{2R_g}{\Delta R_1 + \Delta R_2 + \Delta R_3 + \Delta R_4}} \quad 5-4$$

The equations presented here are the basic bridge equations [Dally, 1984 and 1992]. As seen from equations 5-3 and 5-4, when  $R_g$  is large, the Wheatstone bridge will produce the largest responses as measured by  $\Delta E$ . Note also that a stable source of input voltage,  $V_{INPUT}$ , is needed to ensure consistent measurements.

### 5.2.2 Bridge Configurations

The Wheatstone bridge can be used in three ways. The first is called a null balance system, which is used in this dynamometer design. Initially, the bridge is brought to balance by adjusting the resistances in the arms of the bridge. This may be accomplished by adding variable resistance elements to the bridge. Then, when the gages are strained, the variable resistance elements are further adjusted to produce a balanced system again. The amount of this adjustment is, then, a measure of the change in the strain gage resistance, or the strain. In reality, the dynamometer used in this thesis employs a signal conditioner/amplifier to initially balance the circuitry of the full Wheatstone bridge. Since the forces generated are dynamic in nature, the cutting force is measured continuously for the duration of the cutting. The collected signal is the output voltage of the bridge, and its magnitude is recorded by and determined from the DAQ system.

The second configuration in which a Wheatstone bridge can be used is called the unbalance system. In this case, a computer, a data acquisition board, and software are integrated to form a data acquisition system that is directly connected to the bridge. The bridge output is recorded as a function of time. This system is capable of both static and dynamic strain measurements. As mentioned earlier, a constant source of input voltage is necessary in this system since the output is directly proportional to the strain.

Lastly, the Wheatstone bridge can be used as a reference system. This system incorporates features of both the null balance and the unbalance systems.

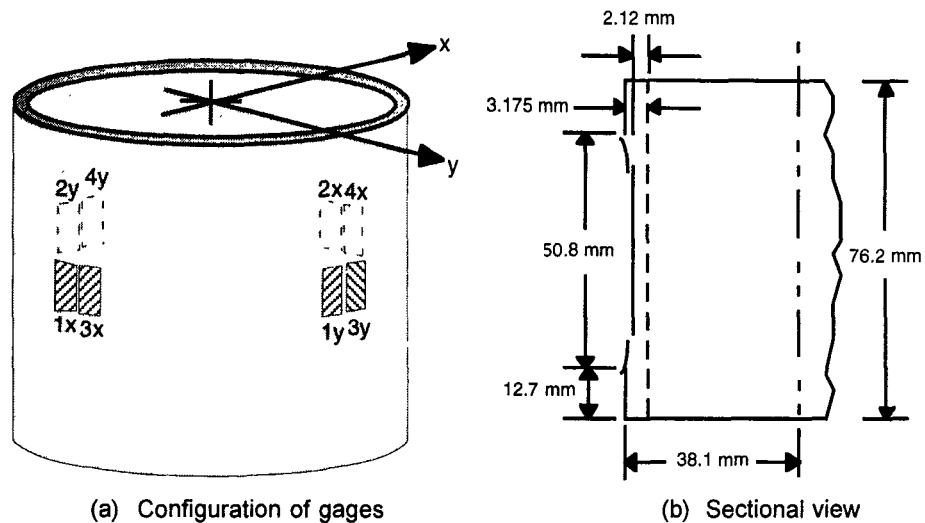
In addition to the strain gage bridge, this system uses another full bridge as a reference. Initially, the reference bridge can be adjusted to cancel the output of the strain gage bridge. Then when the strain gage bridge is strained, the reference bridge is readjusted to match the output of the strain gage bridge. The amount of readjustment is an indication of strain. Or, as in the unbalance system, the reference bridge can be adjusted to yield a balanced overall system output. Any changes recorded afterwards is directly proportional to strain.

### **5.3 SENSING ELEMENT**

One of the most critical components of a dynamometer is the sensing element. The sensing element is that component of the dynamometer that converts the mechanical energy of a physical phenomenon, such as deflection, to strain. For a sensitive dynamometer, the strain must be maximized on the sensing element. Normally, electrical sensors are placed directly on the sensing element to record the strain, as in the case of metal-foil strain gages.

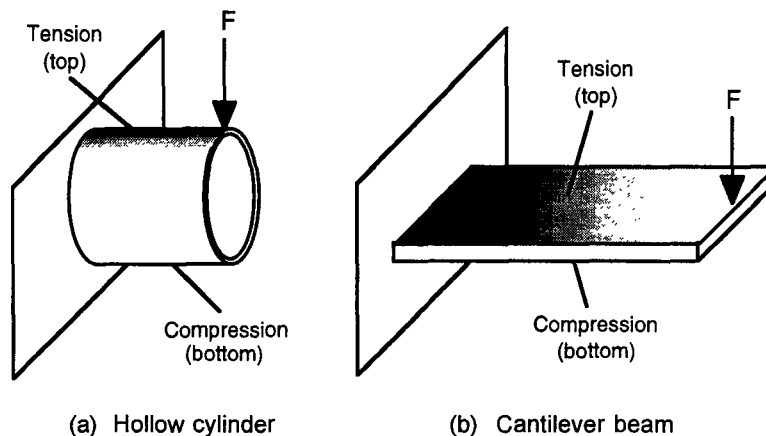
In this dynamometer design, a hollow cylinder is used as the sensing element, as shown in Figure 5-3. Because the cylinder is a highly rigid structure, the thickness of the mid-section is reduced to increase the strain induced on that location during loading. Figure 5-3 (a) indicates the mounting location the strain gages. Figure 5-3 (b) shows that the top and bottom portions of the cylinder have a thickness of 3.125 mm, while the middle portion, which was turned using a lathe, has a thickness of 2.12 mm. Note that the interfaces, where the middle portion of the cylinder surface meets the top and bottom portions, are rounded to eliminate stress concentrations.





**Figure 5-3. Sensing element: (a) strain gage configuration and (b) sectional view**

The use of a hollow cylinder as a sensing element represents a compromise between rigidity and sensitivity because it must not only be rigid enough to support the whole structure, but also be sensitive enough to small deflections. As illustrated in Figure 5-4, the response of the hollow cylinder to an applied force  $F$  can be thought of as being similar to that of a cantilever beam in which tension (shaded areas) and compression act on the top and bottom surfaces, respectively. This



**Figure 5-4. Strain response of (a) a hollow cylinder and (b) a cantilever.**

assumption is based on the fact that the cylinder is rigidly attached (by welding) at one end to a base plate which is clamped to the table of a milling machine. The other end is also welded to a plate but is not supported and carries the weight of the rest of the dynamometer.

In general, it is desirable to have the sensing element as close as possible to the source where the forces are being applied. Otherwise, strain sensitivity is diminished because the full energy of the cutting force during its transmission from component to component may be reduced due to friction and other types of energy losses. Thus, the placement of the strain gages on the sensing element is an important consideration. Depending on how the forces are applied, strain gages can be mounted in several different configurations. In this design, the goal is to measure forces in terms of their planar components, i.e. X and Y directions. Figure 5-3 shows how the strain gages are mounted on the sensing element [Dally, 1993]. Note each strain gage has a counterpart directly opposite on the other side of the sensing element. Thus, for example, when a force is applied to the sensing element in the positive x direction, tension results in gages 1x and 3x, while compression results in gages 2x and 4x. Assuming the y-direction gages (1y, 2y, 3y, and 4y) are

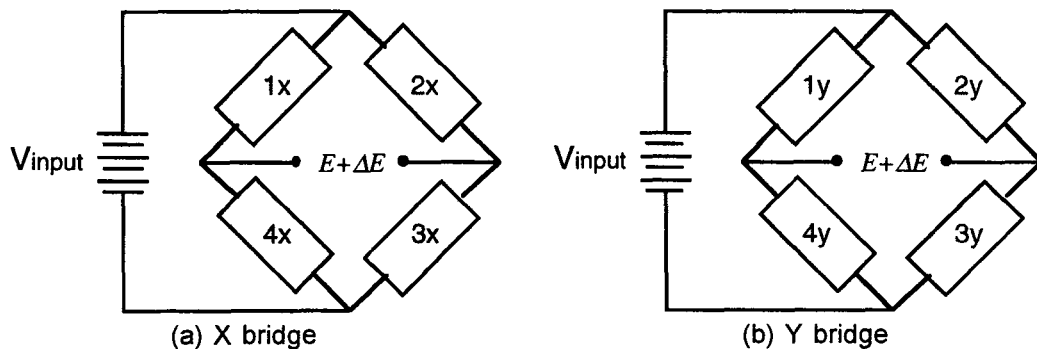


Figure 5-5. The strain gages in Figure 5-3 are shown in their bridge configurations ninety degrees apart from their respective x-gage counterparts, they should not be

stressed since they are located at the neutral axis. When all the gages are connected to form Wheatstone bridges, they measure the force components independently. Figure 5-5 shows how the gages are connected properly.

## **5.4 THE DYNAMOMETER**

Figure 5-6 shows the fully assembled dynamometer in operation during a machining experiment. In the figure, the dynamometer is secured to the table of the milling machine while specimens mounted on a fixture inside the tank are machined by the end mill. During machining, the dynamometer and the table move in the X-Y plane (i.e., the plane parallel to the ground), while the spindle platform moves vertically.

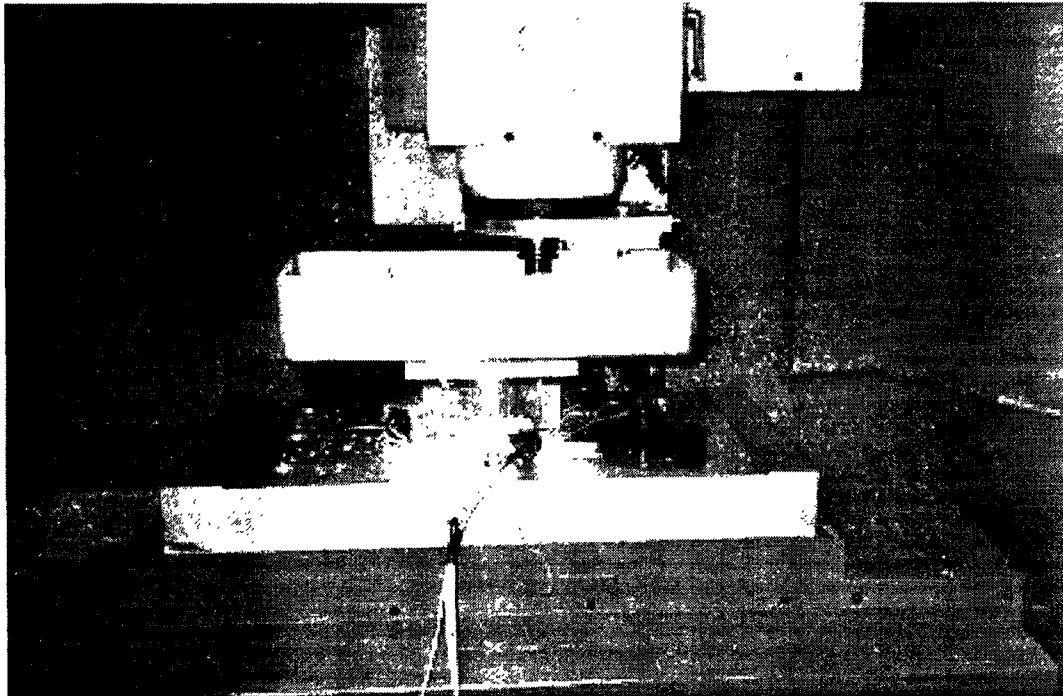


Figure 5-6. Dynamometer shown during a machining experiment

### **5.4.1 Components of the Dynamometer**

The major components of the dynamometer include the base, cylinder, top, tank, a fixture plate, grips, fixture, and a protective unit that guards the strain gages. The overall dimensions of the dynamometer are 48.3 cm long, 19.2 cm wide, and 23.2 cm high, as shown in Figure 5-7. All components are machined from aluminum with the exceptions of the tank, which was ordered, and the protective unit, which was made by a stereolithography machine from a resin material.

A prominent feature of the dynamometer is the tank. Its main function is to hold different cutting lubricants, such as water, alcohol, and oil. The advantage in varying the cutting environment is that it has a direct effect on the surface finish of machined ceramics. Certain lubricants, combined with an optimized set of machining parameters, produce very good surface finish. The tank also serves as a chip collector. Table 5-1 lists the specifications of all the components.

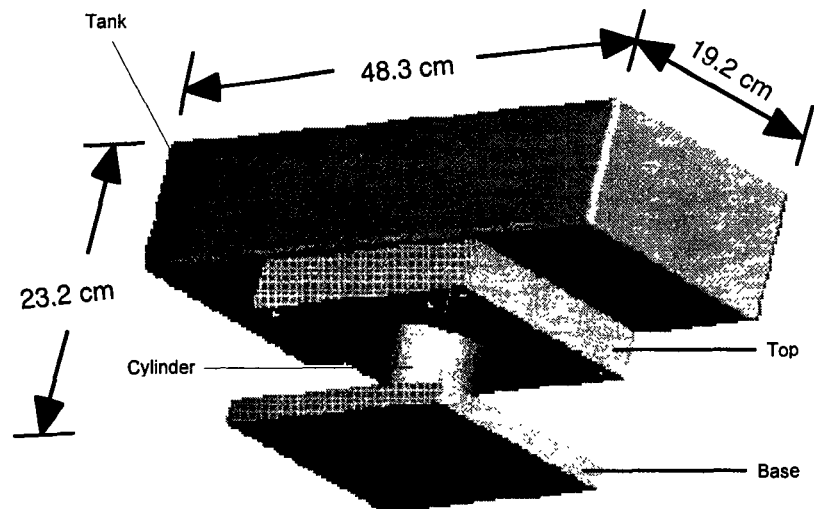
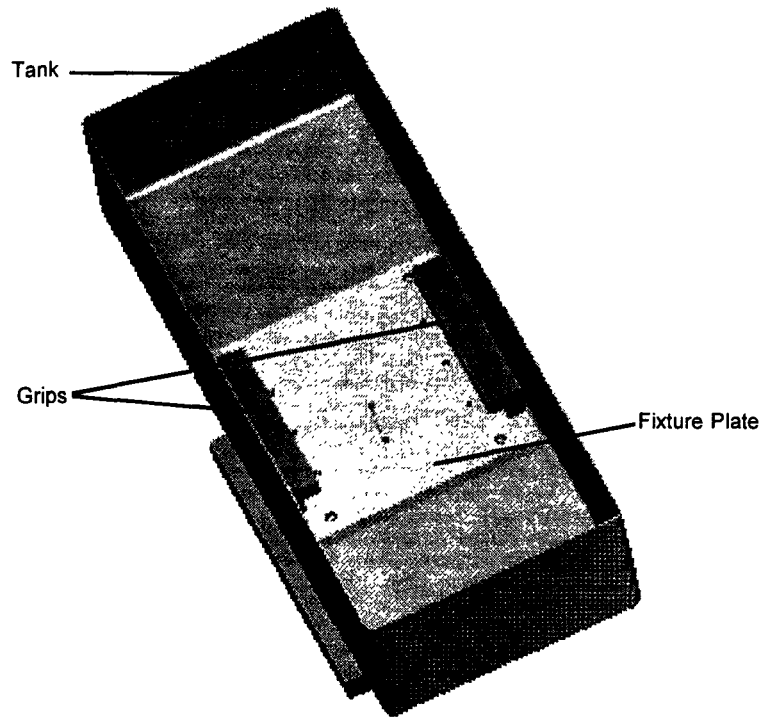


Figure 5-7. Overall dimensions of the dynamometer

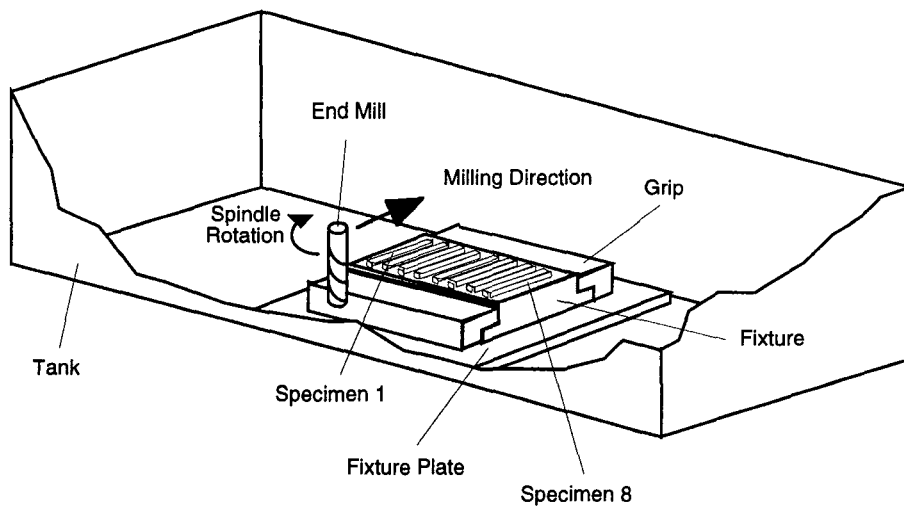
Table 5-1. Components of the dynamometer

| <b>COMPONENT</b> | <b>FUNCTION</b>   | <b>DIMENSIONS</b>           | <b>MASS</b>              |
|------------------|---|-----------------------------|--------------------------|
| Base             | Supports whole structure                                      | 27 cm x 27 cm x 1.8 cm      | 3.1 kg                   |
| Cylinder         | Provides elastic element for strain gages                     | 7.6 cm x 7.6 cm x 0.64 cm   | 0.14 kg                  |
| Top              | Supports tank & rest of components                            | 17.8 cm x 20.3 cm x 1.7 cm  | 1.6 kg                   |
| Tank             | Provides different environments for machining; collects chips | 48.3 cm x 19.2 cm x 10.6 cm | 2.6 kg                   |
| Fixture Plate    | Supports fixture  | 17.8 cm x 14 cm x 1.2 cm    | 0.64 kg                  |
| Grips            | Secures fixture   | 12 cm x 2.5 cm x 2.5 cm     | 0.28 kg (2)              |
| Fixture          | Mounts ceramic specimens for machining                        | 12 cm x 9.5 cm x 2.5 cm     | 0.68 kg                  |
| Protective Unit  | Protects strain gages from physical contact                   | 16.5 cm x 16.5 cm x 5.6 cm  | n/a (light-weight resin) |

In Figure 5-8, the details of the components within the tank are shown. In particular, Figure 5-8 (a) shows the top view of the dynamometer and Figure 5-8 (b) illustrates how the fixture, with specimens mounted, is placed between the grips and on the fixture plate. During machining, the tool with the indicated spindle rotation passes over each specimen in the milling direction as shown. Eight specimens are mounted on the fixture at a time, and each is machined with a unique set of machining conditions according to the factorial design of experiments discussed in the next chapter. Note that the specimens are placed in sequence from 1 through 8 as indicated in Figure 5-8 (b). Furthermore, the design of the fixture plate incorporates a back-stop that locks the fixture at exactly the same position each time the fixture slides in between the grips. To assemble the various components, threaded bolts with washers secure together the grips, fixture plate, tank, and top. The cylinder is welded at both ends to the top and base components.



(a) Top view



(b) Components inside tank

Figure 5-8. Details of the top components of the dynamometer

### 5.4.2 Estimation of the Natural Frequency

To ensure that the dynamometer is capable of measuring the cutting force without interference from its own vibration, the natural frequency of the dynamometer must be known. In general, this requirement is satisfied if the natural frequency of vibration of the dynamometer is at least four times the frequency of the cutting force [Shaw, 1984]. To obtain an estimate of the natural frequency of the dynamometer, the system may be approximated by a mass that is supported by a spring, such as in Figure 5-9. In this system,  $m$  consists of the masses of the top, tank, fixture plate, fixture, and grips. The cylinder is not counted because its mass is negligible. However, its spring constant,  $k$ , represents that of the whole system and is found by assuming the cylinder is a cantilever beam:  $k = \frac{3EI}{l^3}$ , where  $E$  = Young's modulus,  $I$  = moment of inertia, and  $l$  are parameters of the cylinder.

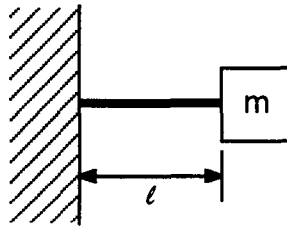


Figure 5-9. Dynamometer represented by spring-mass system

For a hollow cylinder of a small thickness  $t$  and of diameter  $d = (d_{\text{outer}} + d_{\text{inner}})/2$ , the moment of inertia is defined by  $I = \frac{\pi d^3 t}{8}$ . Therefore the natural frequency of the spring-mass system in Figure 5-9 is given by  $f_n = \frac{1}{2\pi} \sqrt{\frac{386.4k}{m}}$  (Hz). Given that  $E = 10 \times 10^6$  psi,  $I = 1.1659 \text{ in}^4$ ,  $l = 3 \text{ in}$ , and  $m = 12.787 \text{ lb}$  for the dynamometer, the calculated natural frequency about 1000 Hz. In the

machining experiments described in Chapter 6, the spindle speeds of the end mill used are 600 rev/min and 900 rev/min, or 10 Hz and 15 Hz, respectively. Thus the ratio of the natural frequency of the vibration of the dynamometer to the frequency of the excitation source, i.e. spindle speed, is well beyond the factor of 4.

## 5.5 DATA ACQUISITION SYSTEM

The purpose of a data acquisition (DAQ) system is to collect data from a physical phenomenon as it varies over time. In this case, the DAQ system is designed to measure the cutting force during the machining of ceramics. Figure 5-10 shows part of the setup of the DAQ system, including a computer running the software LabVIEW and a signal conditioning module, the instrumentation front end for a plug-in DAQ board.

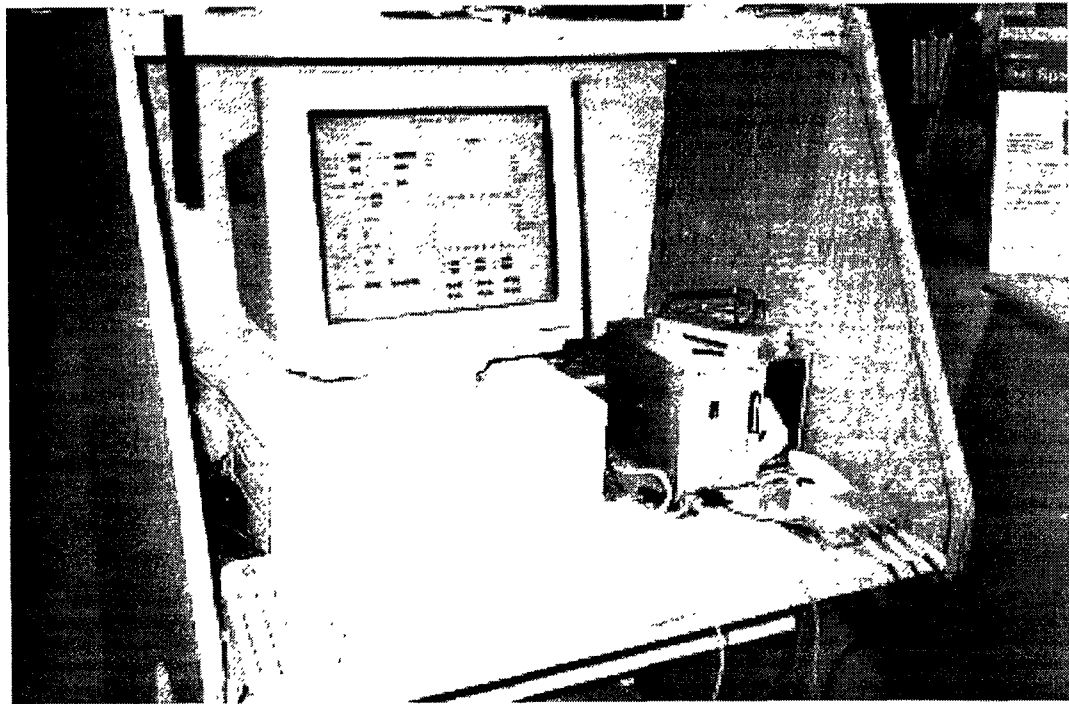
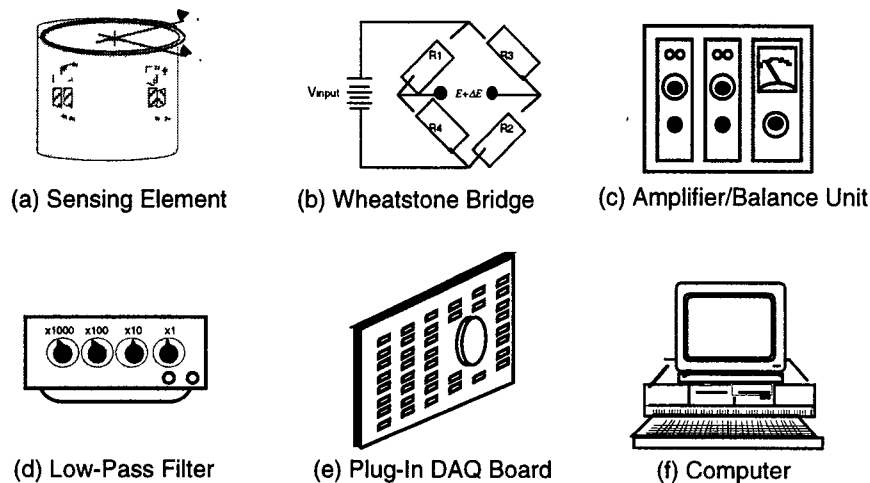


Figure 5-10. Computer with LabVIEW running and signal conditioning module



The complete DAQ system is shown in Figure 5-11. The system starts from the sensing element where deflections are induced by the applied cutting forces. To measure the deflections, strain gages are attached on the surface of the sensing element to form full Wheatstone bridges. The bridges are regulated by an amplifier/balance unit to provide, among other things, voltage input for the bridges to function as electrical sensors, and to record the output voltage signals. Thus, any changes recorded in the output signals are an indication that deflections has occurred in the sensing element. From here, the signals are passed on to a low-pass filter where high-frequency noise in the signals is filtered. Next, the filtered signals are converted from analog to digital format by an analog-to-digital converter (ADC), or DAQ board. Finally, the digitized signal is processed by a software running on a computer where the data can be displayed and/or stored.



**Figure 5-11. Components the data acquisition (DAQ) system**

Table 5-2 lists the specifications of each component in Figure 5-11. Note that the bandwidth of the amplifier/balance unit is 15 kHz, while the DAQ board is 255 kHz. Obviously, the lower value of the amplifier/balance unit is the governing

bandwidth of the DAQ system. In addition, Table 5-2 indicates that the DAQ board has an analog resolution of 16-bit and a maximum sampling rate of 100,000 samples per second.

Table 5-2. DAQ system characteristics

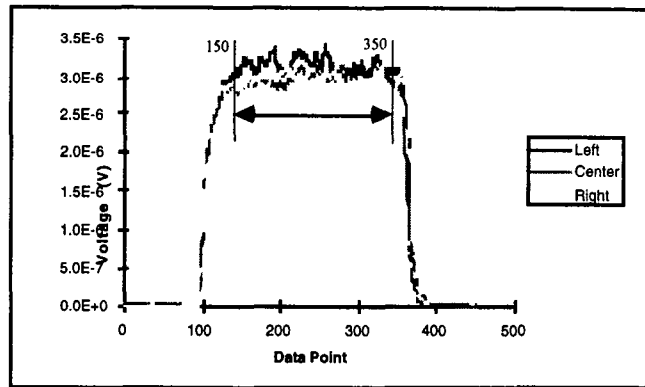
| <b>DAQ SYSTEM CHARACTERISTICS</b>               |   |
|---|---|
| <b>Specification</b>                            | <b>Type/Value</b>                                       |
| <b>Strain Gages</b>                             | Measurements Group<br>CEA-13-250UW-350                  |
| Resistance                                      | 350 ohms  |
| Gage factor                                     | 2.135   |
| Transverse sensitivity                          | 0.5   |
| <b>Wheatstone Bridge</b>                        | Full  |
| Input   | 5 Vdc   |
| <b>Amplifier/ Conditioner/<br/>Balance Unit</b> | Measurements Group<br>2100 System                       |
| Gain  | 1 to 2100   |
| Bandwidth                                       | dc to 15 kHz: - 3 dB                                    |
| Excitation                                      | Const. voltage: 0.5 to 12 Vdc                           |
| Balance   | $\pm 2000 \mu\text{E}$ to $\pm 6000 \mu\text{E}$        |
| <b>Low-Pass Filter</b>                          | Frequency Devices 900                                   |
| Corner Frequency                                | 50 Hz   |
| <b>Plug-In DAQ Board</b>                        | National Instruments<br>AT-MIO-16X                      |
| Analog resolution                               | 16-bit  |
| Max. sampling rate                              | 100 ksamples/sec  |
| Bandwidth                                       | dc to 255 kHz, all gains: -3 dB                         |
| <b>Computer</b>                                 | Pentium PC running LabView<br>from National Instruments |

## 5.6 CALIBRATION

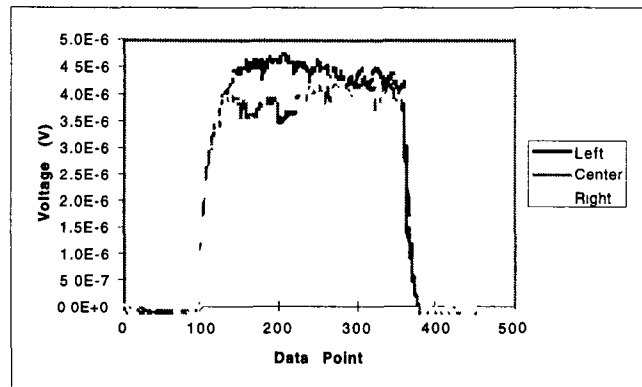
Calibration is the last and most critical stage in the construction of a dynamometer. This is because the dynamometer is sensitive to the location of the applied force. This is because the sensing element of the dynamometer is a cylinder and is subject to torsional effects. Since strain gages are mounted to measure forces applied in the center location on the top of the cylinder, any applied forces not near the center location will induce moments in the cylinder to lessen the measured magnitude of the deflections by the strain gages.

The sensitivity of the dynamometer is further affected by torsion because, due to natural design limitations in metal foil gage, the strain gages have an inherent sensitivity in the transverse direction. As discussed previously, however, the transverse sensitivity is small, only  $(+0.5 \pm 0.2)\%$ . This compares to the gage factor, which measures sensitivity in the direction of the wire axis, of 2.135.

To determine the location sensitivity of the dynamometer, metallic specimens are mounted on the fixture at three different locations -- center, 0.5 inches to the left of center, and 0.5 inches to the right of center -- and machined using identical machining conditions. Figure 5-12 presents the force results. Note that the variation in the feed direction is less than that of the transverse direction. Table 5-3 lists the mean of the cutting forces in Figure 5-12 and compares the deviation of the left and right locations from the center position. These results indicate that the dynamometer is sensitive to the location of the machining specimens, and that care must be taken in calibration.



(a) Feed direction



(b) Transverse direction

Figure 5-12. Plots showing variation of measured cutting forces

Table 5-3. Variation of the cutting force due to specimen location

| Feed Force (V)       |          |                      |
|----------------------|----------|----------------------|
| Location             | Mean     | $\Delta$ from center |
| Left                 | 3.16E-06 | 0.09e-6 (2.9%)       |
| Center               | 3.07E-06 | —                    |
| Right                | 2.95E-06 | 0.12e-6 (3.9%)       |
| Transverse Force (V) |          |                      |
| Location             | Mean     | $\Delta$ from center |
| Left                 | 4.45E-06 | 0.59e-6 (15%)        |
| Center               | 3.96E-06 | —                    |
| Right                | 4.07E-06 | 0.11e-6 (2.8%)       |

Lastly, some calibration data is presented on the dynamometer in Figure 5-13. The calibration is performed on the center location of the fixture. In Figure 5-13 (a), the ratio of the slope of the X response (feed direction) to the slope of the Y response (transverse) is  $(0.023 \text{ V/N}) / (0.007 \text{ V/N}) = 3.3$ . In Figure 5-13 (b), the ratio is  $(0.017 \text{ V/N}) / (0.002 \text{ V/N}) = 8.5$ . Hence, the ratios are greater than 3, an indication that the cross-talking of the dynamometer is adequately small.

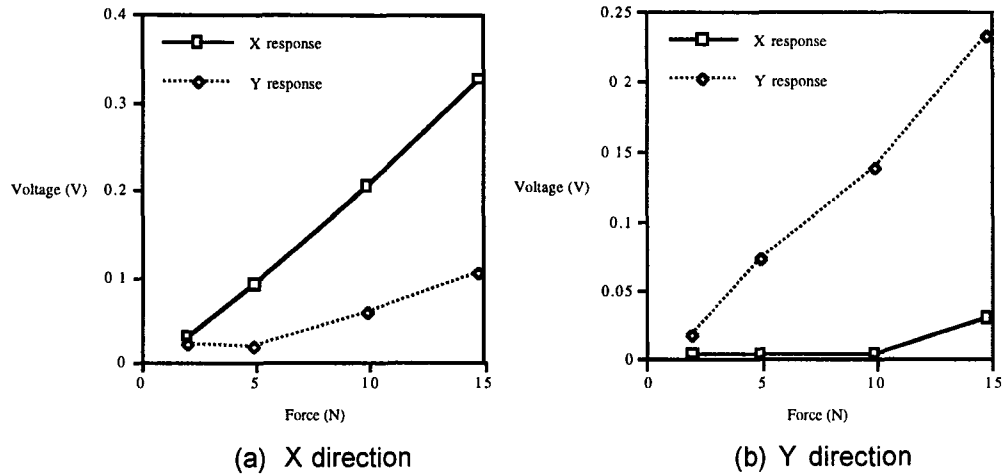


Figure 5-13. Calibration results for the (a) X direction and (b) Y direction

## **Chapter 6**

### **Evaluation of Machining Performance**

The evaluation of machining performance forms a basis for machinability assessment. The evaluation is based on two sets of data. The first set of data is the cutting force measurement, and the second set of data is the measurements of the flexural strength before and after machining. The basic methodology is to determine the degradation of flexural strength due to machining and correlate the degradation to the cutting force produced during machining. To effectively perform the evaluation, a 2-level, 3-variable, full factorial design of experiments is used to relate the parameters of machining to the measured cutting forces and flexural strength. In particular, empirical models are developed to express the relationship of machining parameters to the machining performance. Finally, effects of material microstructure to machining performance are assessed.

#### **6.1 PROCEDURE**

The evaluation of machining performance starts from machining and measuring cutting forces, then to determining flexural strength after machining, and finally to developing mathematical models from collected empirical data. A systematic approach, based on the factorial designs, is used to machine the ceramic materials to ensure that data collected will contain the information needed for the evaluation. The evaluation of machining performance consists of four steps, and are summarized as follows:

1. Machining Experiments: A CNC, three-axis milling machine is used to machine the ceramic materials. A high-speed-steel, 2-flute end mill, 6.35-mm in diameter, is mounted to the milling machine. Machining is performed under dry conditions, i.e. no coolant used.
2. Cutting Force Measurement: Force signals, generated in the feed and transverse directions during material removal, are recorded by a data acquisition system comprising of the dynamometer, a personal computer, and the LabVIEW software.
3. Fracture Strength Evaluation After Machining: Four-point flexural strength tests are performed on all specimens after machining. Pure tension is applied to the machined surface side of each specimens.
4. Data Analysis: Empirical models are developed from the measurements of cutting forces and evaluation of flexural strength after machining. In each model, a  $2^3$  full factorial design is applied to study the main effects, as well as any interaction effects, of the three key machining parameters on the cutting forces and flexural strength.

Regarding the details of the machining experiments, the settings for the spindle speed, feed rate, and depth of cut are derived from the principles of factorial design in which two levels, "high" and "low", denoted by plus (+) and minus (-) signs, respectively, are selected for each parameter. Listed in Table 6-1 are the high and low settings for all three parameters used in this research.

Table 6-1. High and low settings for the machining parameters

| Level    | Spindle Speed<br>(rpm) | Feed Rate<br>(mm/min) | Depth of Cut<br>(mm) |
|----------|------------------------|-----------------------|----------------------|
| High (+) | 900                    | 30                    | 0.19                 |
| Low (-)  | 600                    | 20                    | 0.12                 |

Furthermore, to fulfill the requirements of a 2-level, 3-variable full factorial experiment,  $2^3$ , or eight, tests are performed, with the machining parameters set according to the design matrix shown in Table 6-2. This table shows all of the possible testing combinations for the factorial design. For each of the three DICOR/MGC materials, eight tests, as specified by the design matrix, are conducted; in all, 24 tests are performed.

The design matrix can also be represented geometrically as a cube in which the three dimensions of length, width, and height are defined by the three machining parameters. As illustrated in Figure 6-1, three orthogonal edges of the cube represent the axes of spindle speed, feed rate, and depth of cut. The eight unique tests are represented by eight corners in the cube as listed in Table 6-2.

Table 6-2. Design Matrix

| TEST | VARIABLE      |           |              |
|------|---------------|-----------|--------------|
|      | Spindle Speed | Feed Rate | Depth of Cut |
| 1    | -             | -         | -            |
| 2    | +             | -         | -            |
| 3    | -             | +         | -            |
| 4    | +             | +         | -            |
| 5    | -             | -         | +            |
| 6    | +             | -         | +            |
| 7    | -             | +         | +            |
| 8    | +             | +         | +            |



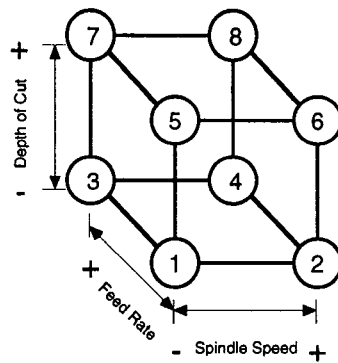


Figure 6-1. Geometrical representation of the design matrix

To carry out the eight tests for each material, a fixture is designed as shown in Figure 6-2. For each ceramic material, a set of eight specimens, as illustrated by the rectangular bars, are secured to a sliding metal fixture by first placing them in slots that have been machined at evenly spaced locations, and secondly, applying epoxy around the specimens to form a strong bond to the fixture. Once the specimens and fixture are secured, machining is performed using a 6.35 mm-diameter end mill with one pass over each specimen. This diameter is chosen to ensure that the end mill machines the whole surface of each specimen with just one pass.

Finally, note that the dynamic force generated from the cutting action of the end mill can be decomposed into its orthogonal directions, the feed and transverse, as illustrated by Figure 6-2. To clarify, the feed force refers to the force component generated in the direction of the path that the end mill travels, while the transverse force is the force component generated in the direction that is 90 degrees from the feed direction. During machining, these two force components are measured simultaneously by the dynamometer.

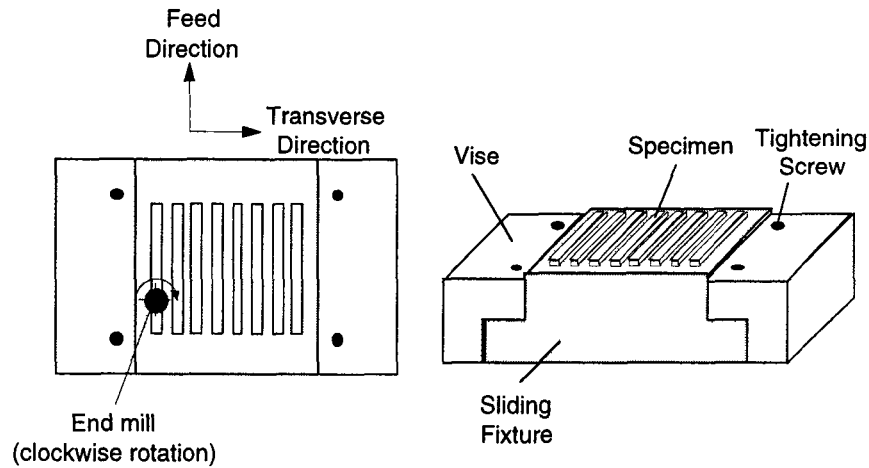


Figure 6-2. Vise-fixture system for machining

## 6.2 EXPERIMENTAL DATA

### 6.2.1 Cutting Forces

An example of a set of recorded cutting force signals is shown in Figure 6-3. In particular, the recorded signals are characterized by a machining duration -- the time elapsed during machining -- as defined by a start and a finish. From the recorded signals, the mean of the cutting force is computed from the absolute value of each data point of the recorded signals. Since the signals are both positive and negative because of the change of force direction, the mean of the data points must be computed from their absolute values; otherwise, it would lead to adding positive and negative values. A better method of obtain the mean is to use the squared value of each data point. However, in establishing the relationship of the force data with the machining conditions, there seems to be no particular advantage in siding with one method over the other.

The signal in Figure 6-3 is recorded at a sampling rate of 300 points per second. In this particular example, a spindle speed of 600 revolutions per min, or 10 Hz, is used so that the sampling rate is adequate. However, it should be pointed out that since there are two flutes on the end mill, it is expected that the frequency of the tool impacting the ceramic is doubled at 20 Hz.

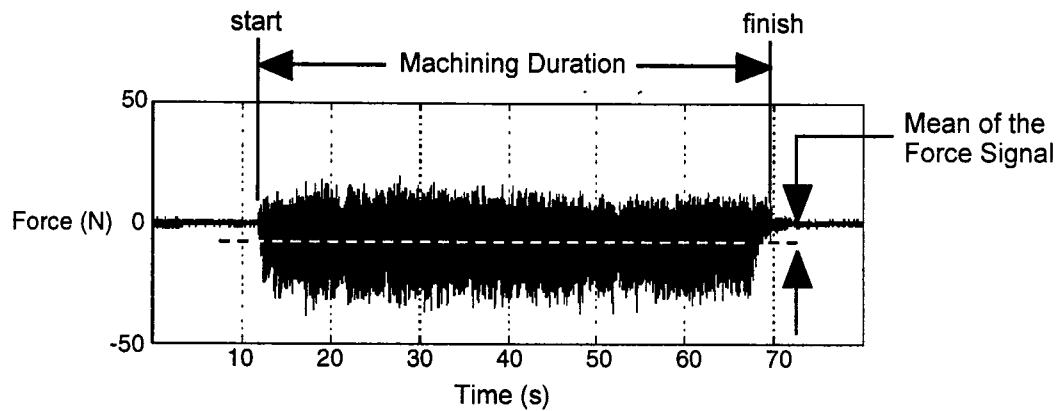


Figure 6-3. Example of a force signal

In Table 6-3, the cutting forces measured by the dynamometer during the machining of the DICOR/MGC materials are listed. For each material, both the feed and transverse forces are listed, along with the settings of the machining parameters. For example, in test #1 of Table 6-3 (a), a fine DICOR specimen is machined with a low spindle speed, a low feed rate, and a low depth of cut. The forces recorded are the feed and transverse forces.

### 6.2.2 Fracture Strength Measurements

After machining, the specimens are released from the metal fixture and are subjected to four-point bending tests, as illustrated in Figure 6-4. The machined surface is shown as indicated. During bending, two forces are applied from the top

to induce tension on the machined surface, which ultimately fracture the specimen when a critical load is reached. Ideally, the fracture should occur between the two inner bars, characterizing that the failure is contributed to pure bending. In this test, a voltage reading,  $V$ , is taken after each fracture, and is converted to a fracture load,  $FL$ , by the following formula [NIST, 1996]:

$$FL = 10 \times (0.32 + 39.79V) \quad 6-1$$

Table 6-3. Cutting Force Measurement Data

a) Fine DICOR/MGC

| Test # | Machining Conditions |           |              | Feed Force [N] | Transverse Force [N] |
|--------|----------------------|-----------|--------------|----------------|----------------------|
|        | Spindle Speed        | Feed Rate | Depth of Cut |                |                      |
| 1      | -                    | -         | -            | 15.59          | 3.05                 |
| 2      | +                    | -         | -            | 2.19           | 0.86                 |
| 3      | -                    | +         | -            | 3.34           | 2.26                 |
| 4      | +                    | +         | -            | 11.98          | 3.46                 |
| 5      | -                    | -         | +            | 1.38           | 2.56                 |
| 6      | +                    | -         | +            | 6.95           | 4.95                 |
| 7      | -                    | +         | +            | 7.44           | 7.37                 |
| 8      | +                    | +         | +            | 3.12           | 3.19                 |

b) Medium DICOR

| Test # | Machining Conditions |           |              | Feed Force [N] | Transverse Force [N] |
|--------|----------------------|-----------|--------------|----------------|----------------------|
|        | Spindle Speed        | Feed Rate | Depth of Cut |                |                      |
| 1      | -                    | -         | -            | 0.53           | 0.39                 |
| 2      | +                    | -         | -            | 2.34           | 3.30                 |
| 3      | -                    | +         | -            | 2.64           | 3.94                 |
| 4      | +                    | +         | -            | 4.86           | 2.94                 |
| 5      | -                    | -         | +            | 5.18           | 6.15                 |
| 6      | +                    | -         | +            | 4.40           | 1.70                 |
| 7      | -                    | +         | +            | 0.88           | 3.34                 |
| 8      | +                    | +         | +            | 3.18           | 5.31                 |

c) Coarse DICOR

| Test # | Machining Conditions |           |              | Feed Force [N] | Transverse Force [N] |
|--------|----------------------|-----------|--------------|----------------|----------------------|
|        | Spindle Speed        | Feed Rate | Depth of Cut |                |                      |
| 1      | -                    | -         | -            | 0.30           | 0.65                 |
| 2      | +                    | -         | -            | 1.83           | 1.63                 |
| 3      | -                    | +         | -            | 2.85           | 3.35                 |
| 4      | +                    | +         | -            | 2.53           | 1.28                 |
| 5      | -                    | -         | +            | 2.94           | 4.33                 |
| 6      | +                    | -         | +            | 2.04           | 0.88                 |
| 7      | -                    | +         | +            | 1.47           | 1.89                 |
| 8      | +                    | +         | +            | 4.54           | 6.70                 |

To get the flexural strength, FS, a final conversion is performed using another equation, defined by [NIST, 1996]

$$FS = 3/4 \times \left( \frac{L}{wd^2} \right) \times FL \quad 6-2$$

In equations 6-1 and 6-2, L and the distance between the top two pins are determined by the calibration of the DAQ system.

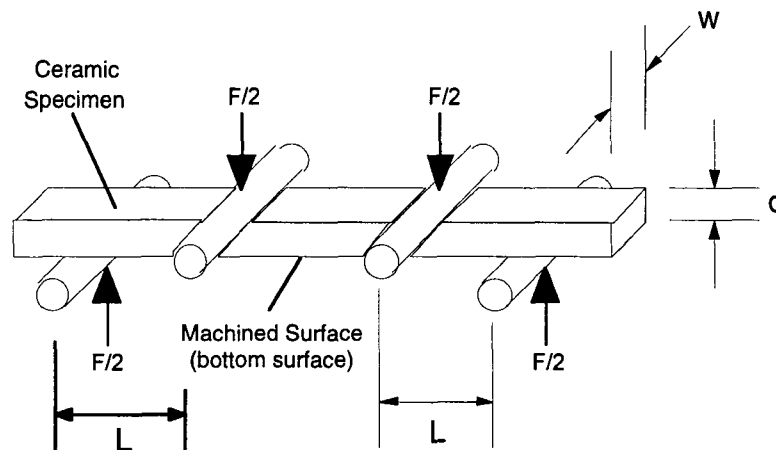


Figure 6-4. Four-Point Bending Tests to Evaluate Fracture Strength

The purpose of the bending tests is to measure the fracture strength of the

DICOR/MGC materials after machining to assess their post-machining performance. The four-point bending tests are performed in parallel to block possible variations introduced to the measurement data. Table 6-4 presents the data obtained from these measurements. The table shows the flexural strengths for each type of material. The "before machining" column refers to the flexural strength as measured from raw material which has not been machined. Conversely, the "after machining" column refers to the flexural strength as measured after the material has been machined.

Table 6-4. Fracture Strength Measurement Data (MPa)

| DICOR/MGC-Fine |                  |                   |            | DICOR/MGC-Medium |                  |                   |            |
|----------------|------------------|-------------------|------------|------------------|------------------|-------------------|------------|
| Test #         | Before Machining | After Machining * | Difference | Test #           | Before Machining | After Machining * | Difference |
| 1              | 260 ± 22         | 47                | 213        | 1                | 225 ± 18         | 41                | 184        |
| 2              | 260 ± 22         | 49                | 211        | 2                | 225 ± 18         | 89                | 136        |
| 3              | 260 ± 22         | 34                | 226        | 3                | 225 ± 18         | 66                | 159        |
| 4              | 260 ± 22         | 47                | 213        | 4                | 225 ± 18         | 34                | 191        |
| 5              | 260 ± 22         | 44                | 216        | 5                | 225 ± 18         | 75                | 150        |
| 6              | 260 ± 22         | 45                | 215        | 6                | 225 ± 18         | 66                | 159        |
| 7              | 260 ± 22         | 41                | 219        | 7                | 225 ± 18         | 62                | 163        |
| 8              | 260 ± 22         | 31                | 229        | 8                | 225 ± 18         | 62                | 163        |

| DICOR/MGC-Coarse |                  |                   |            |
|------------------|------------------|-------------------|------------|
| Test #           | Before Machining | After Machining * | Difference |
| 1                | 145 ± 30         | 90                | 55         |
| 2                | 145 ± 30         | 87                | 58         |
| 3                | 145 ± 30         | 86                | 59         |
| 4                | 145 ± 30         | 93                | 52         |
| 5                | 145 ± 30         | 91                | 54         |
| 6                | 145 ± 30         | 83                | 62         |
| 7                | 145 ± 30         | 97                | 48         |
| 8                | 145 ± 30         | 93                | 52         |

\* After machining data represents one specimen per test; therefore, no range is reported.

### 6.3 DATA ANALYSIS AND DISCUSSION OF RESULTS

### 6.3.1 Relation Between Cutting Force And Strength Degradation

Examining the cutting force data presented in Table 6-3, the three maximum cutting force components of feed force are 15.59 Newtons, 5.18 Newtons, and 4.54 Newtons for the DICOR/MGC-Fine, DICOR/MGC-Medium, and DICOR/MGC-coarse materials, respectively. These three maximum force components were measured when machining the DICOR/MGC-Fine at low spindle speed, low feedrate, and low depth of cut, machining DICOR/MGC-Medium at high spindle speed, high feedrate, and low depth of cut, and machining the DICOR/MGC-coarse at high spindle speed, high feedrate, and high depth of cut, respectively. Using the information and examining the data listed in Table 6-4, the corresponding fracture strengths of these specimens after machining can be identified as 47 MPa for the DICOR/MGC-Fine, 75 MPa for the DICOR/MGC-Medium, and 93 MPa for the DICOR/MGC-coarse, respectively. Figure 6-5 (a) is the plot of these observation together with the fracture strengths measured from those specimens without being machined. Therefore, the plot clearly depicts the magnitudes of strength degradation for the three cases. The largest drop in fracture strength is 213 MPa associated with the DICOR/MGC-Fine, and the least drop is 47 MPa. Here the conclusion is the larger the cutting force component in the feed direction is generated, the severe degradation of the fracture strength can be anticipated.

The second observation is related to the data analysis of the cutting force components in the transversal direction. Figure 6-5 (b) is the plot of the cutting force components in the transversal direction corresponding to the three maximum

cutting force components of feed. They are 3 Newtons, 6 Newtons, and 6 Newtons for the DICOR/MGC-Fine, DICOR/MGC-Medium, and DICOR/MGC-coarse materials, respectively. The variation among the three values is 3 Newtons, which is rather smaller than the variation among the three cutting force components in the feed direction, which is 11 Newtons. From comparing the two variations, it is evident that the dramatic drop of the fracture strength degradation of the DICOR/MGC-Fine material is mainly due to the presence of a significant large value of the cutting force component in the feed direction, which is 16 Newtons. This observation is important because it indicates the possible existence of a threshold stress value, above which cracking will be initiated and propagated in a much faster rate during machining. It is important to point out that using the magnitude of cutting force components in the transversal direction may not be as sensitive as using the component in the feed direction in evaluating the fracture strength degradation.

The third observation from this study is "how to assess the machinability among the DICOR/MGC-Fine, DICOR/MGC-Medium, and DICOR/MGC-coarse materials?" The data presented in this paper could lead readers to think that the DICOR/MGC-Coarse material possesses the best machinability because the fracture strength of the material in its final stage, or after being machined, remains at the highest level when compared to those associated with the DICOR/MGC-Fine and DICOR/MGC-Median materials. However, the machining conditions explored in this study are very limited. Further investigations to look at the machining performance under machining conditions different from what has been used are imperative. In addition, interplay between the grain size and the machining condition applied is so complicated that DICOR/MGC materials with various grain



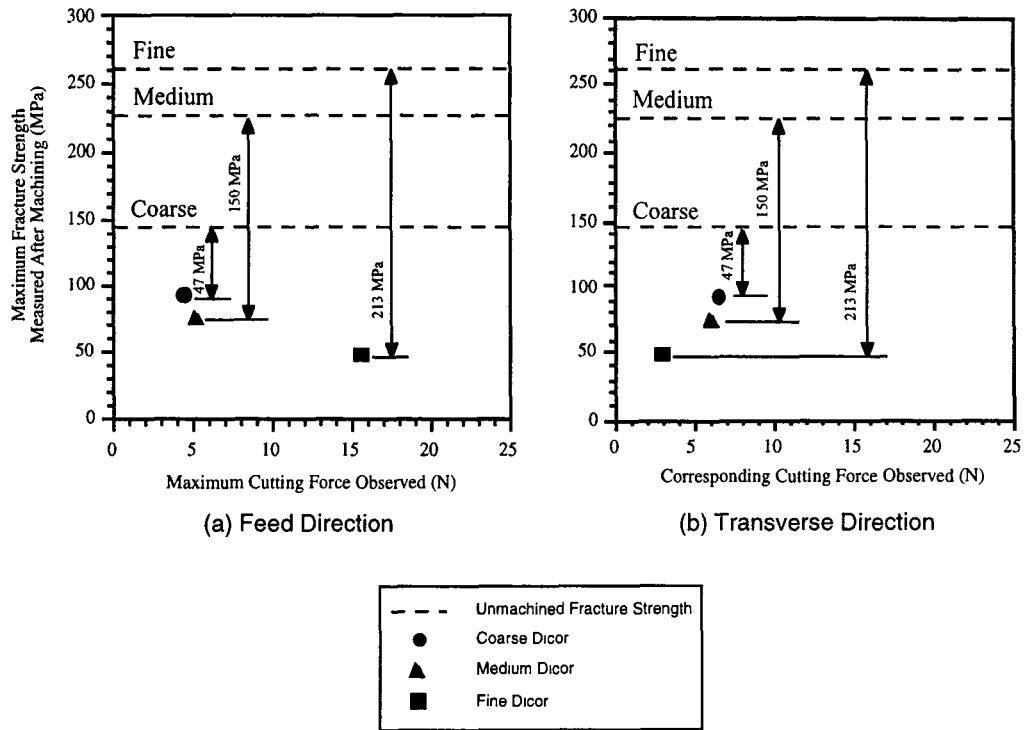


Figure 6-5. Fracture strength degradation of three types of DICOR/MGC for the a) feed and b) transverse directions

sizes, especially between 5  $\mu\text{m}$  to 10  $\mu\text{m}$  in platelet sizes, are needed to further search those machining conditions, under which higher strength levels could be reached, as the data seems to support.

### 6.3.2 Empirical Models Relating the Cutting Force to Machining Conditions

With the observations of the cutting force and flexural strength established in the previous section, empirical models for the cutting force and flexural strength are presented next. The empirical models are based on the main and interaction effects as listed in Table 6-5. In the table, the subscript numbers 1, 2, and 3 refer to the spindle speed (S), feed rate (F), and depth of cut (D), respectively. To form the

relationships, the mathematical model associated with a  $2^3$  factorial design is used. The model is defined as the linear combinations of the machining parameters as follows:

$$F = b_0 + b_1x_1 + b_2x_2 + b_3x_3 + b_{12}x_1x_2 + b_{13}x_1x_3 + b_{23}x_2x_3 + b_{123}x_1x_2x_3 \quad 6-3$$

Table 6-5. Main and interaction effects of machining parameters on the cutting force

a) Feed Direction

| MATERIAL         | E <sub>0</sub> | E <sub>1</sub> | E <sub>2</sub> | E <sub>3</sub> | E <sub>12</sub> | E <sub>13</sub> | E <sub>23</sub> | E <sub>123</sub> |
|------------------|----------------|----------------|----------------|----------------|-----------------|-----------------|-----------------|------------------|
| DICOR/MGC fine   | 6.50           | -0.88          | -0.06          | -3.55          | 3.04            | 1.50            | 1.17            | -7.98            |
| DICOR/MGC medium | 3.25           | 1.89           | 0.28           | 0.32           | 1.37            | -1.13           | -3.04           | 0.17             |
| DICOR/MGC coarse | 2.31           | 0.85           | 1.07           | 0.87           | 0.53            | 0.24            | -0.56           | 1.46             |

b) Transverse Direction

| MATERIAL         | E <sub>0</sub> | E <sub>1</sub> | E <sub>2</sub> | E <sub>3</sub> | E <sub>12</sub> | E <sub>13</sub> | E <sub>23</sub> | E <sub>123</sub> |
|------------------|----------------|----------------|----------------|----------------|-----------------|-----------------|-----------------|------------------|
| DICOR/MGC fine   | 3.46           | -0.70          | 1.22           | 2.11           | -0.80           | -0.20           | 0.31            | -2.49            |
| DICOR/MGC medium | 3.38           | -0.14          | 1.00           | 1.48           | 0.63            | -1.10           | -0.60           | 2.58             |
| DICOR/MGC coarse | 2.59           | 0.07           | 1.43           | 1.72           | 1.30            | 0.61            | 0.26            | 2.83             |

In equation 6-3,  $F$  is the response of the model, and the  $x_1$ ,  $x_2$ , and  $x_3$  are the machining parameters of spindle speed, feed rate, and depth of cut, respectively. The coefficients in the equation,  $b_1$ , ...,  $b_{123}$ , are related to the effects listed in Tables 6-5 by  $b = E/2$ ; and  $b_0$  is the average of the responses, or  $E_0$ .

Applying the model to the results in Tables 6-5, the following equations are derived for DICOR/MGC-fine (results for medium and fine are analogous):

$$F_{\text{feed}} = 6.50 - 0.44S - 0.03F - 1.78D + 1.52SF + 0.75SD + 0.59FD - 3.99SFD \quad 6-4(a)$$

$$F_{\text{transverse}} = 3.46 - 0.35S + 0.61F + 1.06D - 0.40SF - 0.10SD + 0.16FD - 1.25SFD \quad 6-4(b)$$

Here,  $F_{\text{feed}}$ , and  $F_{\text{transverse}}$  are the feed and transverse force responses; and S, F, and D represent the high (+1) and low (-) levels of the spindle speed, feed rate, and depth of cut, respectively. In equations 6-4, note that some of the coefficients are relatively small compared to the first term, or the average response, in each equation. In such cases, the effects of the parameters associated with those coefficients may be negligible due to random variations during the machining experiments. A standard treatment of determining whether an effect is significant is the use of a normal probability plot. To do so, Table 6-6 lists the data points for the normal probability plot for DICOR/MGC-Fine for the feed force.

Table 6-6. Data points for normal probability plot for DICOR/MGC-Fine

| DICOR/MGC-Fine (Feed Force) |                        |                     |                            |
|-----------------------------|------------------------|---------------------|----------------------------|
| Order No., i                | Effect Estimates $E_i$ | Identity of Effects | Cumulative Probability (%) |
| 1                           | -7.98                  | 123                 | 7.1                        |
| 2                           | -3.55                  | 3                   | 21.4                       |
| 3                           | -0.88                  | 1                   | 35.7                       |
| 4                           | -0.06                  | 2                   | 50                         |
| 5                           | 1.17                   | 23                  | 64.3                       |
| 6                           | 1.50                   | 13                  | 78.6                       |
| 7                           | 3.04                   | 12                  | 92.9                       |

The cumulative probability is calculated by

$$p_i = \frac{100(i - 1/2)}{2^3 - 1}, i = 1, 2, \dots, (2^3 - 1)$$

Results for the DICOR/MGC-medium and DICOR/MGC-coarse can be obtained similarly.

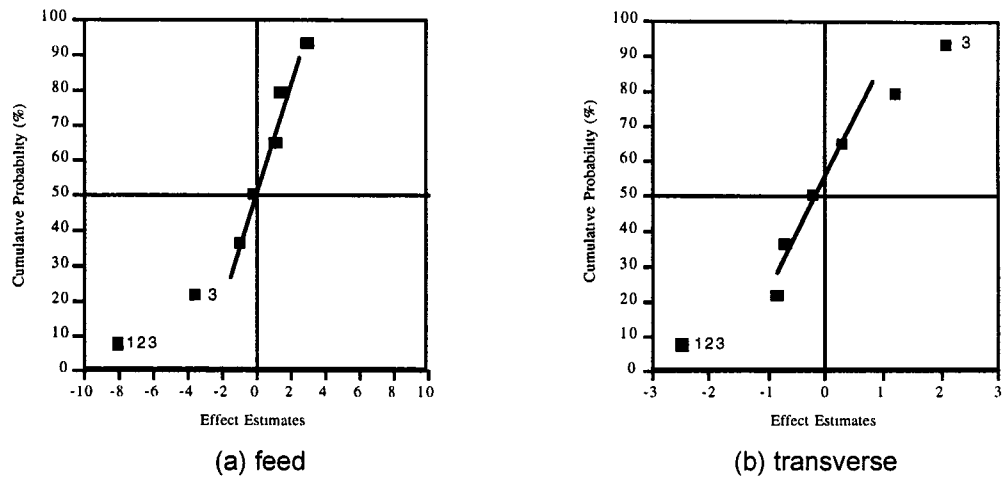


Figure 6-6. Normal probability plot for DICOR/MGC-Fine

The usefulness of these empirical equations is that they serve as starting points in the search for optimized machining conditions that may yield satisfactory machining performance in terms of cutting force and flexural strength. For example, since it was shown in the previous section that the feed component of the cutting force has a more prominent effect on the flexural strength degradation after machining, a good optimization scheme would be to focus on the feed force.

It should be noted here that the relationships developed here are extracted from empirical data, and, because of this, any interpretation of the equations is limited to the range of the input, namely the high and low levels. Therefore, the results are restricted to a very narrow region, and insight into machining performance must be tempered. Furthermore, the statistical significance of these results would be improved if the experiments could be repeated. However, due to scarce resources, this was not possible.

### 6.3.3 The Effects of Microstructure on Cutting Forces, Flexural Strength and Surface Integrity

It should be clear now that the machining performance of the three DICOR/MGC materials are drastically different. Naturally, the question arises as to the underlying cause. As pointed out in Chapter 4, the microstructure of ceramics is very important to the mechanical and physical behavior. Therefore, it is no surprise that the DICOR/MGC, based on three different microstructures in terms of grain size, should perform as they do.

Table 6-7 lists the average forces and flexural strengths recorded for the three DICOR/MGC materials. The average force and strength data referred to here represent the average response of the whole cube of eight tests. For example, the average feed force of 6.5 N for DICOR/MGC-Fine in Table 6-8 is the average of all the feed forces measured in the machining of the eight DICOR/MGC-Fine specimens. Thus, the feed force of 6.5 N can be thought of as a function of  $S$ ,  $F$ , and  $D$ . In this case,  $S = 750$  rpm,  $F = 25$  mm/min, and  $D = 0.155$  mm.

Regarding the forces in Table 6-7, note that as the grain size is increased from fine ( $1.1\ \mu\text{m}$ ) to medium ( $3.7\ \mu\text{m}$ ) to coarse ( $10\ \mu\text{m}$ ), the feed component decreases in a dramatic way. On the other hand, the increase in grain size has very little effect on the transverse component, again, showing that the transverse component of the force is insensitive to different microstructures. As for the flexural strength, it is increased as the grain size is increased. These trends are shown in Figure 6-7.

Table 6-7. 8-test averages and standard deviations from force and flexural strength measurements of DICOR/MGC

| DICOR/MGC | Force (N) |      |            |      | Flexural Strength (MPa) |       |
|-----------|-----------|------|------------|------|-------------------------|-------|
|           | Feed      |      | Transverse |      | Avg.                    | Std.  |
|           | Avg.      | Std. | Avg.       | Std. |                         |       |
| Fine      | 6.50      | 5.07 | 3.46       | 1.96 | 42.25                   | 6.52  |
| Medium    | 3.00      | 1.75 | 3.38       | 1.84 | 61.88                   | 17.55 |
| Coarse    | 2.31      | 1.24 | 2.59       | 2.08 | 90.00                   | 4.50  |

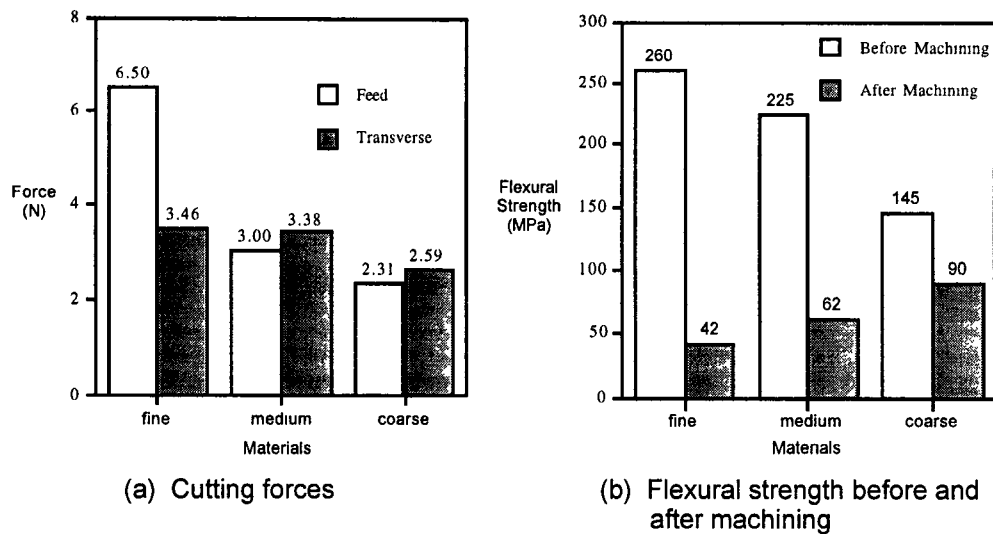


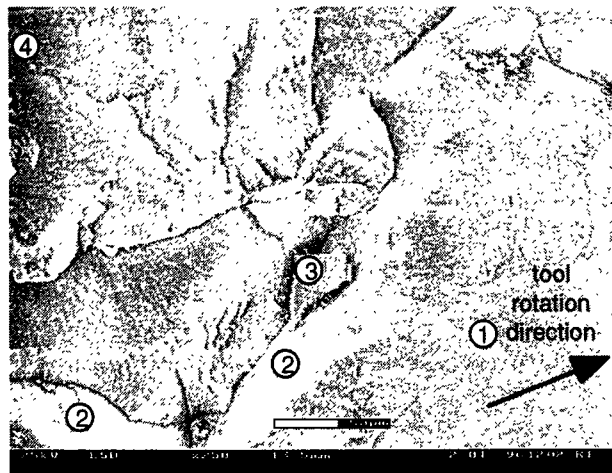
Figure 6-7. Variation of (a) cutting forces and (b) flexural strength degradation as a function of microstructure

Based on these results, it seems that optimization of machining performance is critically dependent not only on the machining parameters, but also on the microstructure of a material. The results seem to support the conclusion that large-grained DICOR/MGC facilitates the mechanism of material removal better than small-grained DICOR/MGC in terms of reducing cutting force generated during machining and of diminishing the flexural strength degradation after machining. Furthermore, it would seem that the small-grained DICOR/MGC is more fracture resistant due to its microstructure, but that the consequences are increased cutting

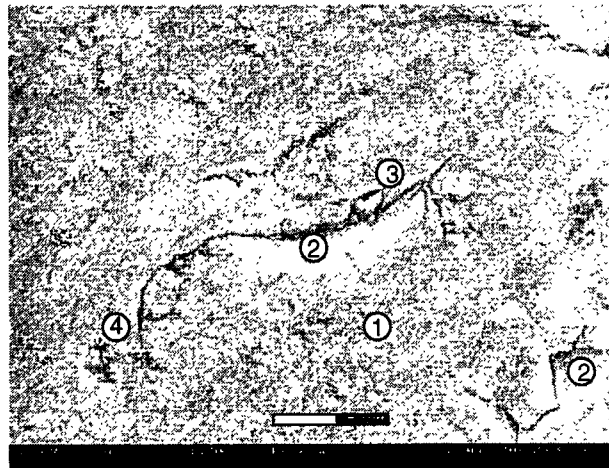
forces, more surface damage, and reduced flexural strength after machining.

As a further example of the effects of microstructure on the machining performance, an examination of the machined surfaces of DICOR is necessary. In Figure 6-8, the fine, medium, and coarse materials are shown. These micrographs are typical of the types of surface features generated after machining. In Figure 6-10 (a), the fine material shows some interesting features. First, note that on the lower right side of the micrograph, the surface is relatively smooth and even (1). Contrasting this is the large volumes being removed (2), caused by the chip-forming process, an example of which is shown in (3). Finally, note the cracking that occurs ahead of the chip-forming process, as evidenced by (4). Assessment of these features suggests that the material removal mechanism by which the fine material operates is one of crack propagation that results in large chip formation when several cracks meet to form the chip volume. However, the force required to propagate the cracks is high, which in turn generates high mechanical stress on the surface. Consequently, the result is uncontrollable fracturing and severe surface damage. This type of damage is consistent with DICOR/MGC-Fine.

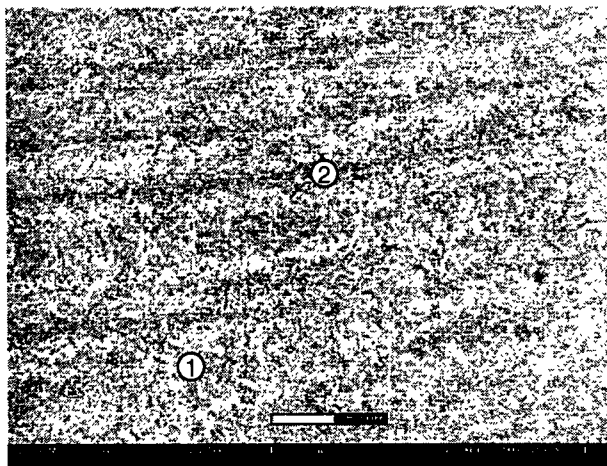
Figure 6-8 (b) is a micrograph of a surface of a machined DICOR/MGC-Medium. Compared to the previous micrograph, one major difference is noticeable: the surface shows tracks left by the cutting tool (1), an indication that the material removal mechanism is somewhat less brittle. However, cracking that leads to brittle fracture is still the primary mechanism, as evident by the large volumes removed (2), brought about by chip formation (3) due to the propagation of cracks (4).



(a) Fine



(b) Medium



(c) Coarse

Figure 6-8. ESEM micrographs (x 250) of machined DICOR/MGC surfaces



Lastly, Figure 6-8 (c) shows the machined surface of DICOR/MGC-Coarse. The micrograph is clearly different from the previous two in that there is no noticeable cracking and chip formation (1). In fact, of the three materials, this material is most ductile-like because its machined surface shows very prominently the tracks left from the cutting tool (2). This is because the material removal mechanism of the coarse material is unlike that of the fine and medium materials. Figure 6-9 is a micrograph of higher magnification of the machined coarse material showing individual grains, which have been sheared in half.

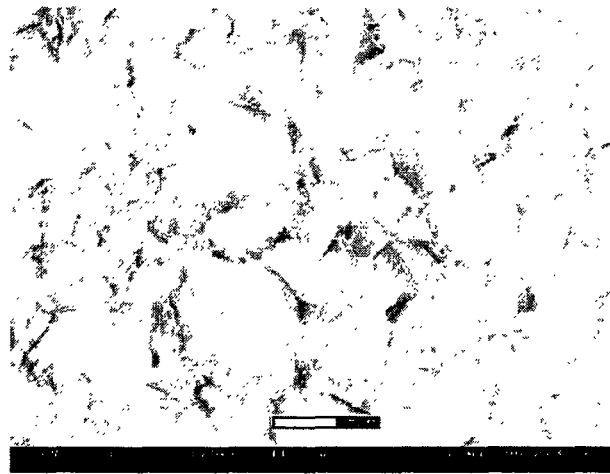


Figure 6-9. Micrograph of DICOR/MGC-Coarse showing material removal mechanism

This is in fact the most likely mechanism of material removal mechanism in the coarse material. The grain-shearing phenomenon can best be described as transgranular cracking that leads to brittle fracture of the individual grains. From this perspective, then, it is easy to understand how the coarse material is the more machinable of the three. It seems that the underlying principle governing the material removal mechanism of DICOR/MGC-Coarse is still cracking and brittle fracture; however, the mechanical stress that induces the failure is less because the

cracking propagates through the grains and not through a tortuous path as may be the case with DICOR/MGC-Fine and DICOR/MGC-Medium. Since cracking is transgranular, subsurface damage is minimized and the flexural strength after machining is not so drastically reduced.

In summary, results obtained from this study clearly indicate that microstructural characteristics of dental ceramics have dominant effects on their mechanical properties, thus leading to a variation of the response of the material to the machining process. To optimize the clinical performance of dental ceramics, a balance has to be made between the effort in material synthesis and the effort in identifying appropriate machining conditions to achieve the minimized strength degradation with a sufficiently high strength sustained after machining.

# **Chapter 7**

## **Conclusions and Recommendations**

### **7.1 CONCLUSIONS**

The overall goal of this thesis has been to study the response of the dental ceramics to the milling process. This thesis presents results obtained from microstructural analysis, machining experiments, and tests to evaluate mechanical properties on DICOR/MGC with three different types of microstructural characteristics: fine, medium, and coarse. Contributions of this these work and significant findings from this study are summarized as follows:

1. Microstructural Analysis. It is common knowledge that material properties depend on their chemical composition and their microstructure. Concentration on the origin of the structure and its influence on the properties and machining performance is the central concept of this study. Thus the work completed in this thesis has been important in understanding the implications of material properties on machining performance.
2. Understanding of Material Removal Mechanism(s). Although the undirected empiricism in processing ceramic material has greatly diminished during the past decade, a comprehensive understanding of the material removal mechanism(s) has not been reached. The material removal mechanisms observed from this study are characterized by

- (1) Intergranular and transgranular crackings. The DICOR/MGC material is characterized by a two-phase structure combined with porosity. These two phases are a crystalline phase of micaceous crystals and a glass phase. It is well accepted that the material removal begins with the crack initiation. Due to mismatched orientations of the crystallines of neighboring grains, grain boundaries are candidates for becoming sites of high stress concentration. Consequently, the cracks are initiated at the bond between the ceramic particles and the glass binder during the machining process. As the machining process continues, the crack propagation progresses. The propagation along the grain boundaries is characterized as intergranular cracking, and the propagation across the grains is characterized as transgranular cracking.
  
- (2) Micromechanisms of material removal. Two types of material removal mechanisms have been identified in this study. The first type is discrete microcrack-based. During machining, microcracks are formed to dislodge individual grains in the process of intergranular cracking along the grain boundaries. These microcracks are also formed due to the fracture of large and elongated grains in the process of transgranular cracking. The second material removal mechanism is the cleavage fracture of coalesced grain arrays. Instead of separation on an individual grain basis, a group of grains is separated at the same time. The characteristics of microstructure, the grain size, shape and the

boundaries, play a dominant role in controlling the material removal mechanisms. For DICOR with fine grains, the cleavage fracture of coalesced grain arrays dominates the chip formation process because of the enhancement of short-crack toughness. For DICOR with large grains, the dislodging of individual grains is the dominant mechanism of material removal.

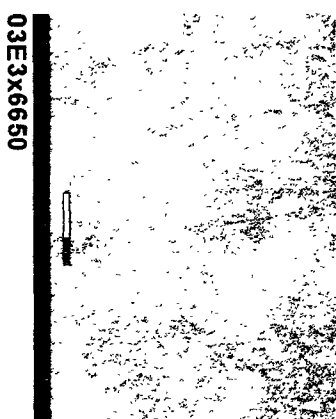
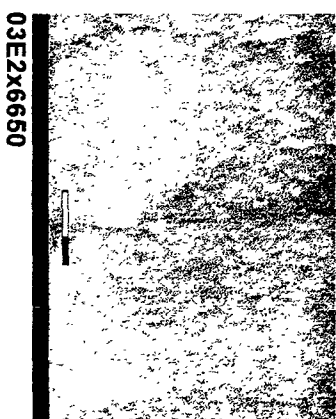
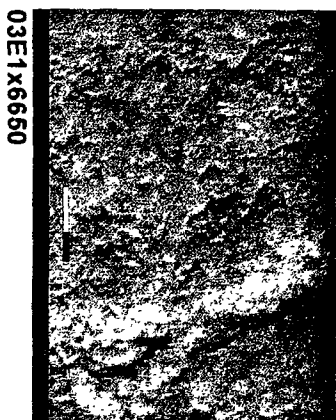
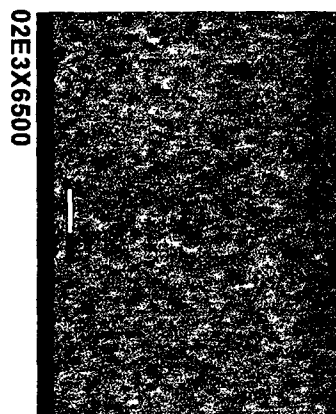
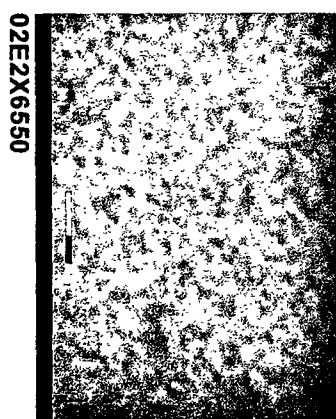
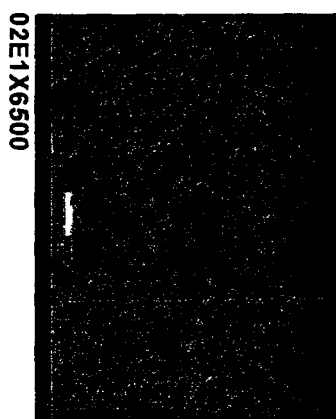
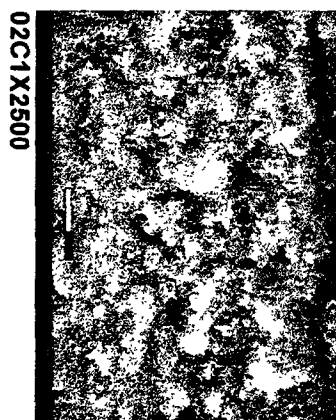
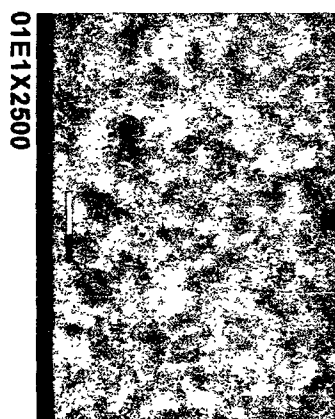
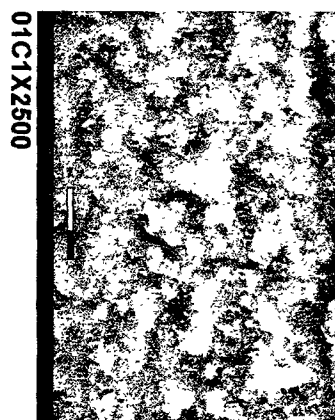
3. Optimization of Machining Performance. The focus of this portion of the work is to determine a viable range to control the strength degradation during machining, since having dental ceramics with high strength is a desired goal. The work started in this thesis provides the lead to further investigations.
4. The dynamometer design completed in this thesis research is successful in measuring the cutting force produced during machining. A balance has been well maintained for maximizing the rigidity of the mechanical structure and achieving an acceptable sensitivity of measurement. Due to the availability of hardware and software, a high-performance data acquisition system has been assembled.

## **7.2 RECOMMENDATIONS**

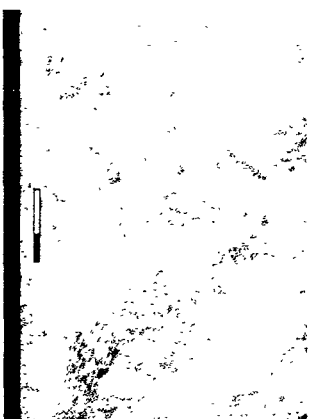
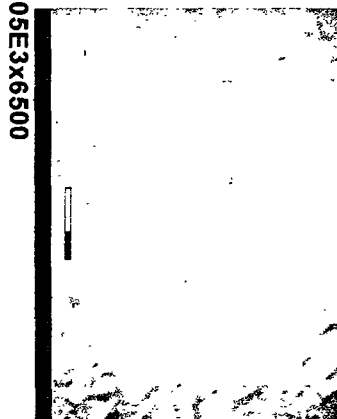
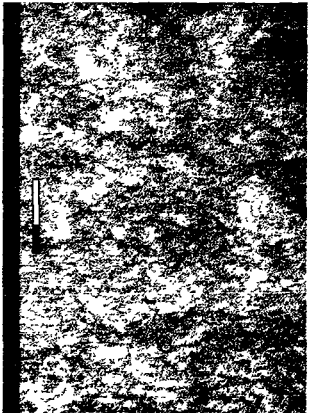
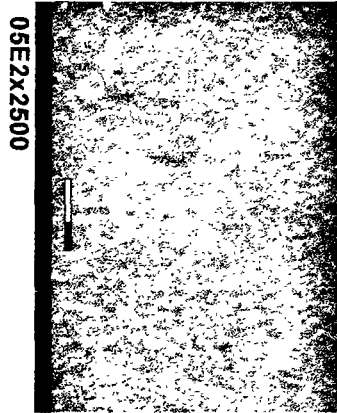
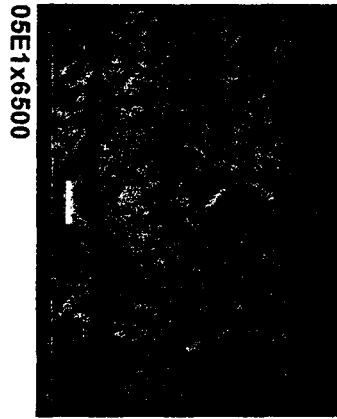
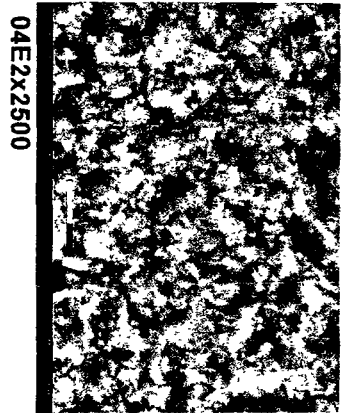
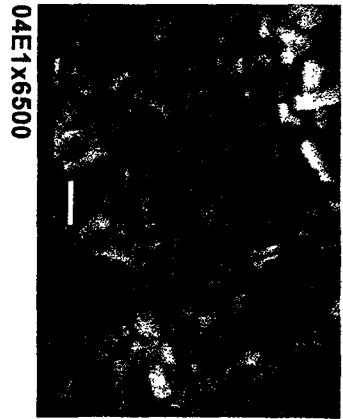
In any ambitious endeavor, methodologies and approaches can always be further improved. This thesis is no exception. In that regard, then, the following recommendations are suggested:

1. The factorial design of machining experiments should be duplicated. By repeating the experiments at individual sites, natural variation of the system response can be more accurately estimated. Furthermore, other factorial designs should be explored to investigate the possibility of non-linearity in the chosen high and low levels.
2. In this study, three micaceous crystal sizes have been studied. DICOR/MGC of other grain sizes should be further explored. A possible size range is between 3.7  $\mu\text{m}$  and 10.0  $\mu\text{m}$ . It is expected that better machining performance can be achieved while reducing the fracture strength degradation.
3. Since surface/sub-surface damage is critical to the reliability of dental restorations, non-destructive evaluation methods should be developed to detect them during machining. Acoustic emission measurements may be one of the candidates for this endeavor.
4. There are several other dental ceramics that exist in the market today. Machining investigation of these other materials is needed for a comprehensive search of the best material.









## **Appendix B**

### **ESEM Micrographs of Machined DICOR/MGC**



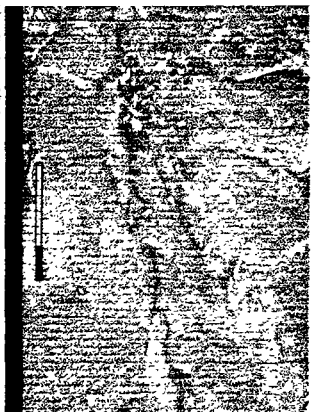
01F1x150



01F1x250



01F1x2500



01F1x500



01F2x100



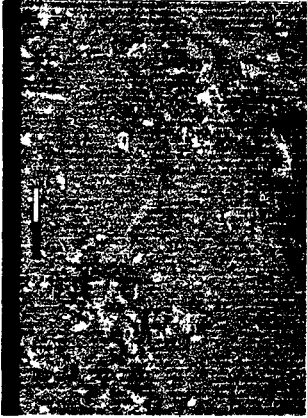
01F2x250



01F2x500



02F1x250



02F1x500



03F1x250



03F1x500



04F1x250



04F1x500



05F1x250



05F1x500



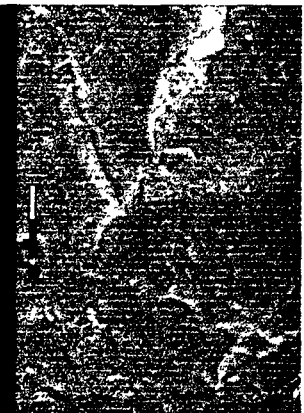
06F1x250



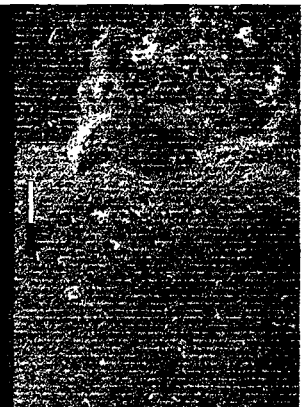
06F1x500



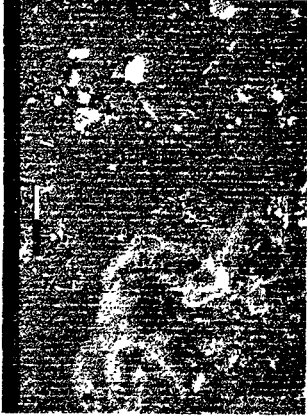
07F1x250



07F1x500



08F1x250



08F1x500



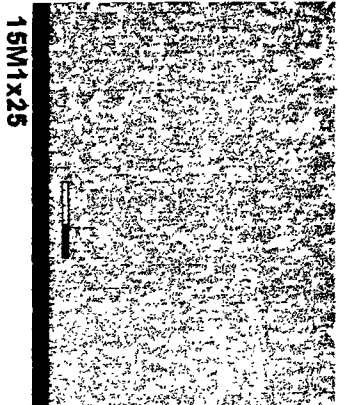
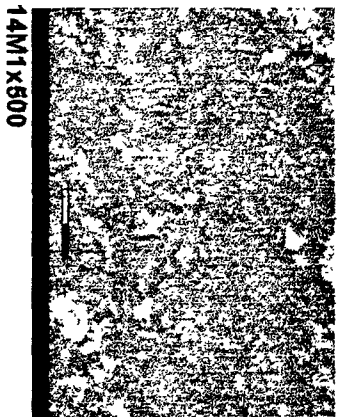
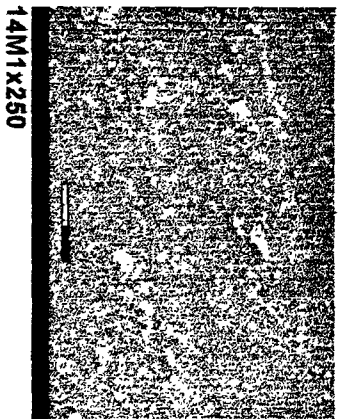
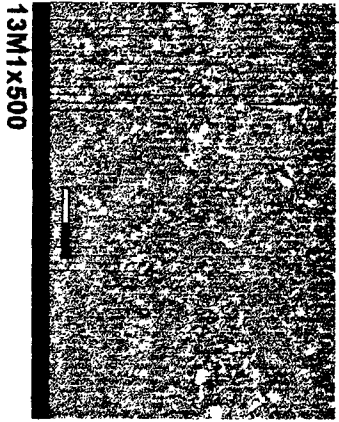
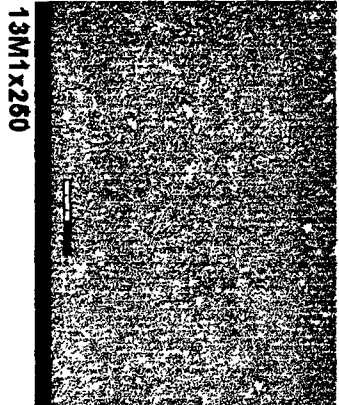
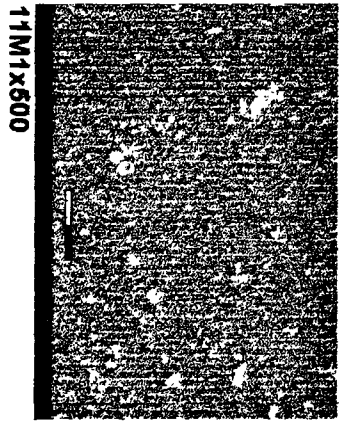
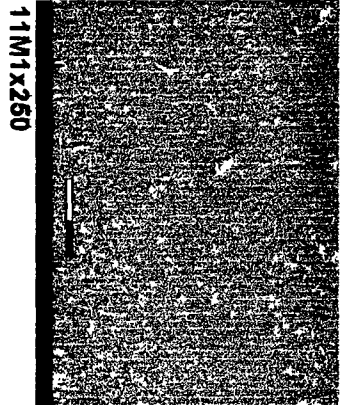
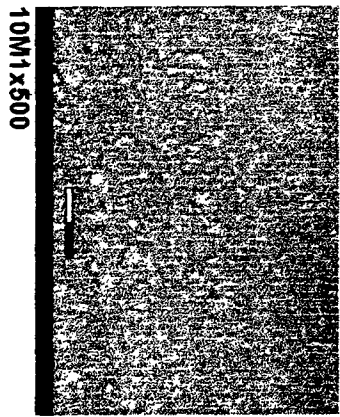
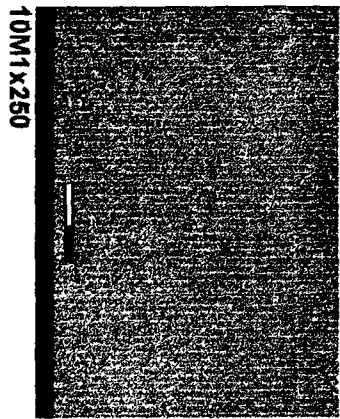
09M1x250



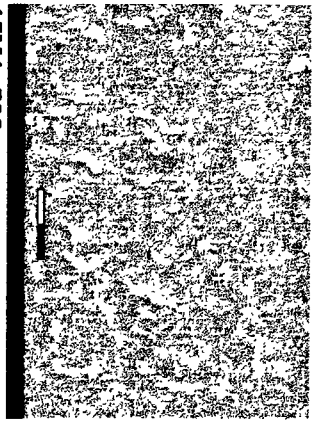
09M1x500



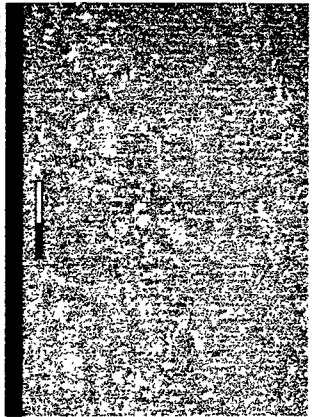
09M2x250



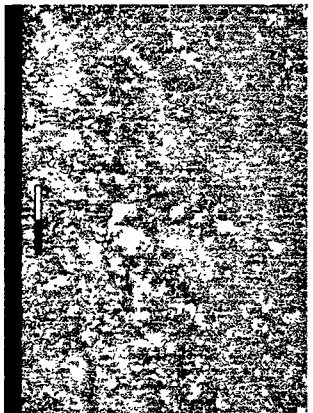




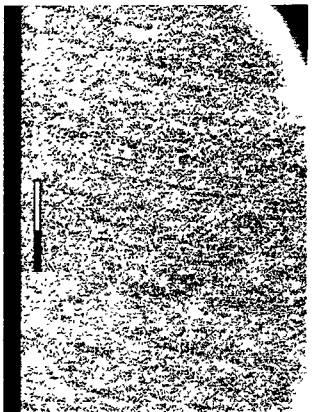
15M1x500



16M1x250



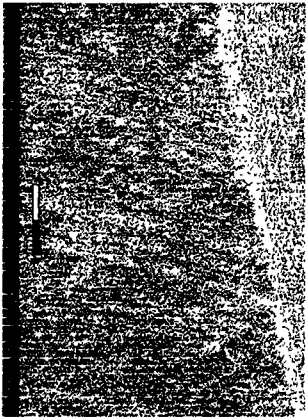
16M1x500



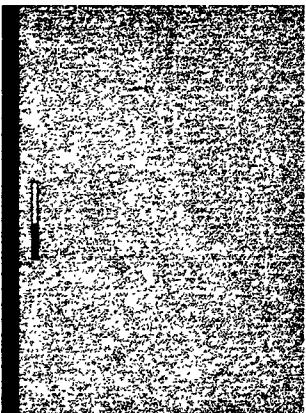
17C1x150



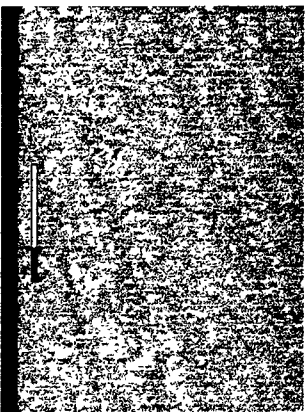
17C1x205



17C1x205b



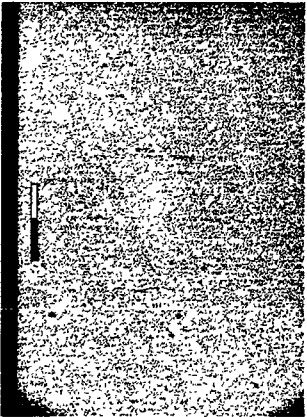
17C1x250



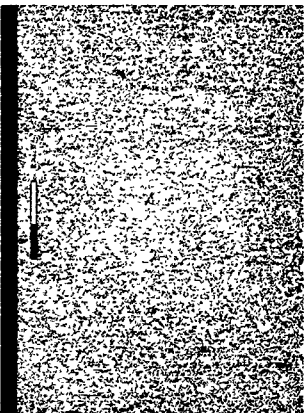
17C1x500



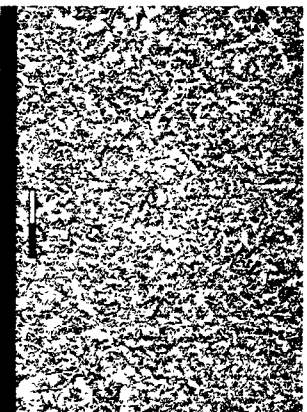
17C1x2500



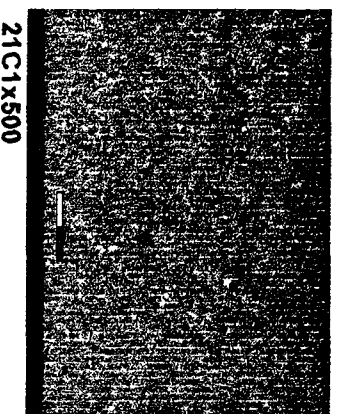
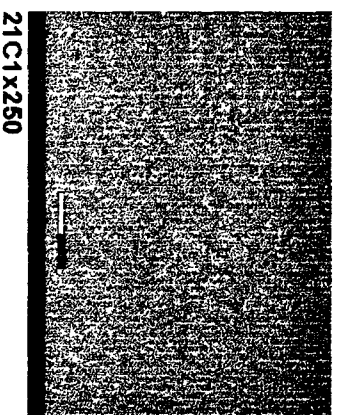
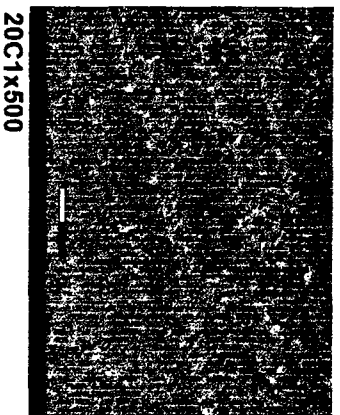
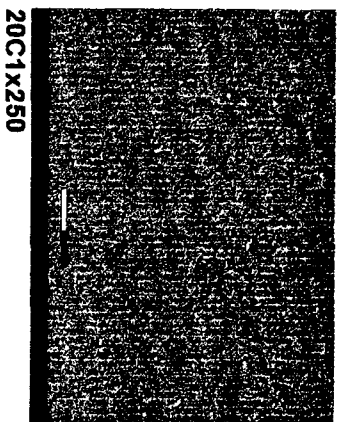
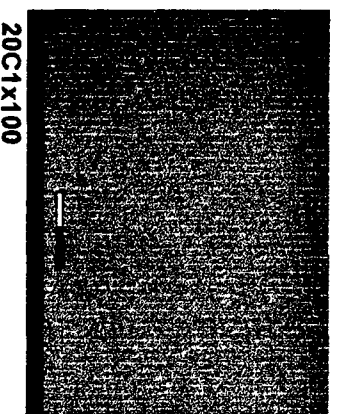
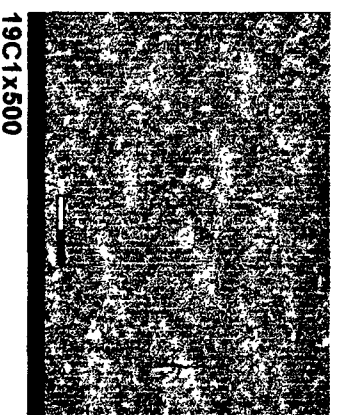
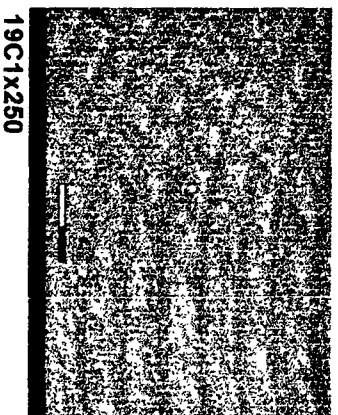
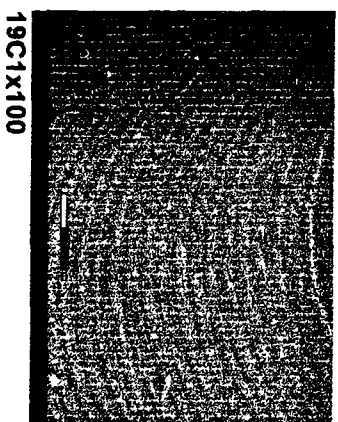
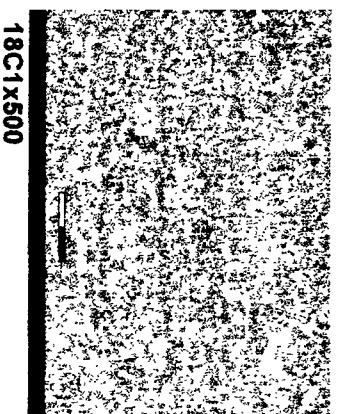
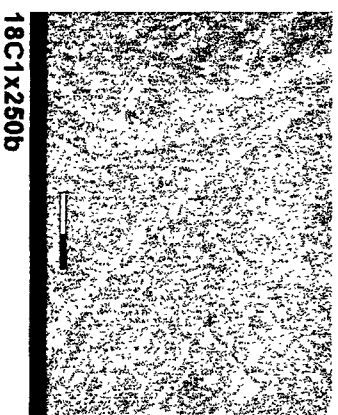
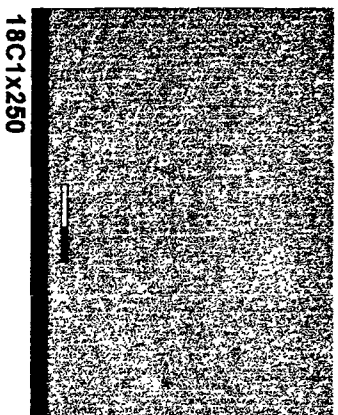
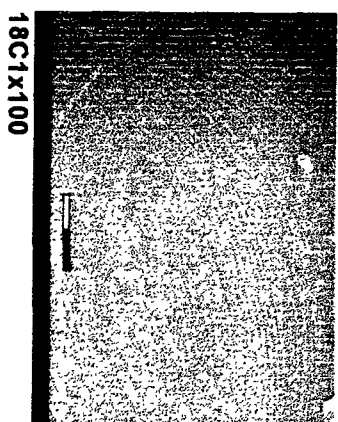
17C2x100

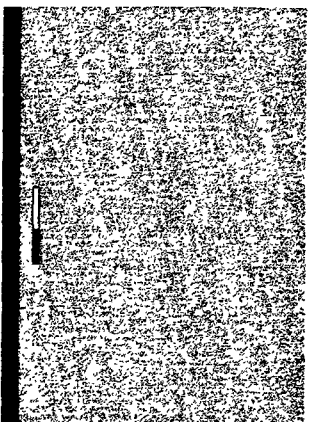


17C2x250

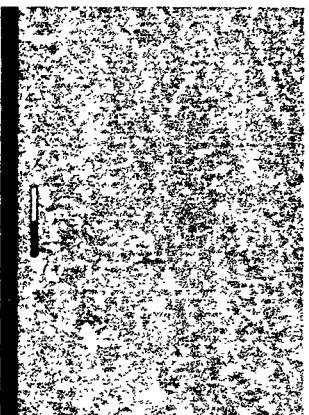


17C2x500

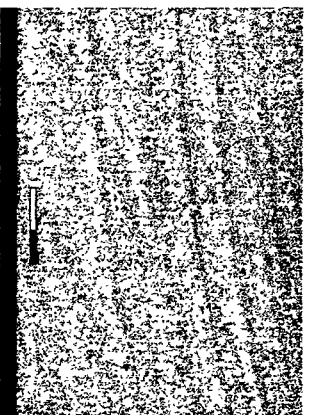




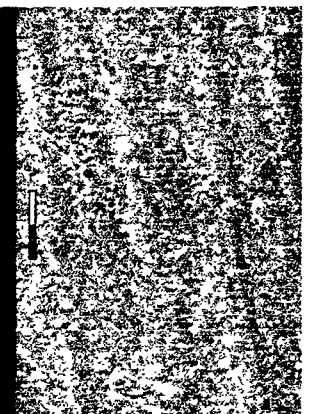
22C1x250



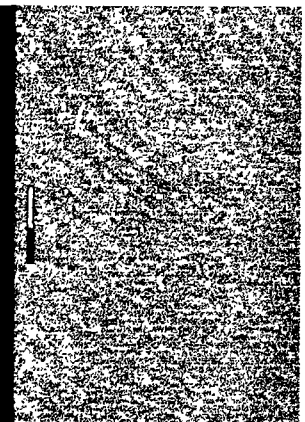
22C1x500



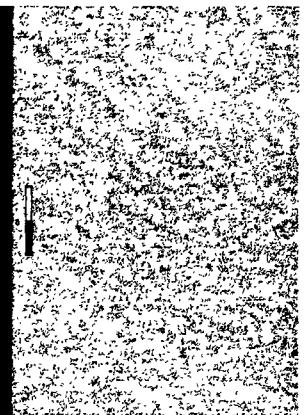
23C1x250



23C1x500



24C1x250



24C1x500



## References

- Bilfano, T. G. and Hosler, J. B., "Precision Grinding of Ultra-Thin Quartz Wafers", Precision Machining: Technology and Machine Development and Improvement, Winter Annual Meeting of ASME, 1992.
- Box, G., W. Hunter, and J. Hunter, "Statistics for Experimenters, An Introduction to Design, Data Analysis, and Model Building." John Wiley & Sons, Inc., 1978.
- Bray, A., Barbato, G., and Levi, R., *Theory and Practice of Force Measurement*, Academic Press Limited, London, 1990.
- Chang, T-C., Wysk, R., and Wang, H-P, *Computer-Aided Manufacturing*, Prentice-Hall, Inc., New Jersey, 1991.
- Evan, A.G., and Marchall, D. B., "Wear Mechanisms in Ceramics," In Fundamentals of Friction and Wear, Ed. D. A. Rigney, Metals Park, Ohio, American Society of Metals, 1980, pp. 439-452.
- Giordano, R. A., "Dental Ceramic Restorative Systems", Compendium, Vol. 17, No. 8, 1996.
- Goldstein, J., Newbury, D., and Echlin, P., *Scanning Electron Microscopy and X-Ray Microanalysis*, Plenum Press: New York, Second Edition, 1992.
- Groenou, B., Maan, N., and Veldkamp, J., "The Science of Ceramic Machining and Surface Finish," edited by B. Hockey and R. Rice, National Bureau of Standards, SP-562, P. 43, 1979.
- Grossman, D. G.: Tetrasilicic mica glass-ceramic material, Washington, D.C.: US Patent Office, US Patent No. 3,732,087, 1973
- Hwang T. W., "Analysis of Surface Quality in Machining of Metals and Advanced Ceramics", Ph.D. Thesis, University of Maryland at College Park, 1992.
- Inasaki, I., "Grinding of Hard and Brittle Materials," Annals of the CIRP, Vol. 36 (2), 1987.
- Ismail, F., et al., "Generation of Milled Surfaces Including Tool Dynamics and Wear", Journal of Engineering for Industry, Vol. 115, 1993.
- Jahanmir, S., Ives, L., and Ruff, A., Ceramic Machining: Assessment of Current Practice and Research Needs in the United States, National Institute of

- Standards and Technology, Report SP-834, 1992.
- Job, L. S., "Assessment of Surface Integrity of Machined Ceramics Using Image Processing", Master Thesis, University of Maryland, 1995.
- Kalpakjian, S., *Manufacturing Processes for Engineering Materials*, Second Edition, Addison-Wesley Publishing Co., Inc., 1992.
- Konig, W., et al, "Machining of New Materials," *Processing of Advanced Materials*, Vol. 1, 1991, pp. 11-26.
- Kulkarni, N. M., Chandra, A., and Jagdale, S. S., "A Dynamic Model for End Milling Using Single Point Cutting Theory", *Journal of Manufacturing Science and Engineering*, American Society of Mechanical Engineers, 1996.
- Lawn, B., *Fracture of Brittle Solids*, Second Edition, Cambridge University Press, 1994.
- Le, D., Lixun, Q., and Zhang, G., "Microstructural Effects on the Machining Performance of Dental Ceramics," Submitted to ASME Mechanical Engineering International Congress and Exposition, 1997.
- Loehman, R. E., Editor., *Characterization of Ceramics*, Butterworth-Heinemann, 1993.
- MATLAB: High Performance Numerical Computation and Visualization Software, The MATH WORKS, Inc., 1992.
- Measurements Group, *Measurements Group Technical Notes*, Measurements Group, Raleigh, North Carolina, 1989.
- Mills, B. and Redford, A. H., *Machinability of Engineering Materials*, Applied Science Publishers, 1983.
- Murray, W. M., and Miller, W. R., *The Bonded Electrical Resistance Strain Gage*, Oxford University Press, Inc., New York, 1992.
- Musikant, Soloman, *What Every Engineer Should Know About Ceramics*, Marcel Dekker, Inc., New York, NY, 1991.
- Ng, S. J., "Machinability Evaluation of Dental Restorative Materials through Surface Texture Characterization", Master Thesis, University of Maryland, 1996.

- Ng, S., Le D. , Tucker S., Zhang G., "Characterization of Machined Induced Edge Chipping in Glass Ceramics," Accepted to present at the 1996 ASME Winter Annual Meeting.
- NIST: National Institute for Standards and Technology, Machinable Ceramics Grant research report, 1996.
- Rekow, D., Zhang, G., and Thompson, V., "Machining Ceramic Materials for Dental Restorations," Proceedings of the International Conference on Machining of Advanced Materials, Maryland, July, 1993, pp. 425-435.
- Satish, K. G., "An Investigation of the Mechanics in the Machining of Ceramic Material", Master Thesis, University of Maryland at College Park, 1994.
- Shaw, M. C., *Metal Cutting Principles*, Oxford University Press, 1984.
- Smith, G. T., *Advanced Machining: The Handbook of Cutting Technology*, IFS Publications, 1989.
- Subramanian, K. and Ramanath, S., "Mechanism of Material Removal in the Precision Grinding of Ceramics", Precision Machining: Technology and Machine Development and Improvement, Winter Annual Meeting of ASME, 1992.
- Wachtman, J. B., *Mechanical Properties of Ceramics*, John Wiley & Sons, Inc., 1996.
- Williams, R., Editor, *Machining Hard Materials*, Society of Manufacturing Engineers, Dearborn, Michigan, 1982.
- Zhang, G., Ko, W., and Ng, S., "Submerged Precision Machining of Ceramic Material," 1995 ASME Conference on Advanced Material Processing, Los Angeles, July 1995.
- Zhang, G., Ng S., Le D. , Tucker S., Rekow D., "Three Dimensional Characterization of Indentation Impressions in Human Enamel", Submitted for Review to the Journal of Dental Materials.
- Zhang, G., Ng S., Le, D., "Characterization of Surface Texture Formed During Machining of Ceramics", Technical Papers of the North American Manufacturing Research Institution of SME, pp. 57-62, 1996.
- Zhang, G., Ng, S., and Le, D., "Assessment of Non-Linear Dynamics of Material Removal on Surface Integrity", to be published in *Dynamics and Chaos in*

*Manufacturing Processes*, John Wiley & Sons, Inc., New York, 1997.

Zhang, G., Satish, K., and Ko, W., "The Mechanics of Material Removal Mechanisms in the Machining of Ceramics," ASME Winter Annual Meeting Proceedings, November 1994, pp. 121-135.